Marine and Petroleum Geology 165 (2024) 106869

Contents lists available at ScienceDirect

Marine and Petroleum Geology

journal homepage: www.elsevier.com/locate/marpetgeo

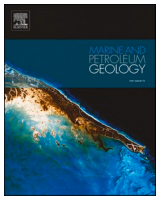

Downslope variability in deep-water slope channel fill facies and stacking patterns

Benjamin G. Daniels [a,b,*], Stephen M. Hubbard [b], Lisa Stright [c], Brian W. Romans [d]

[a] Department of Earth and Environmental Sciences, Mount Royal University, 4825 Mount Royal Gate SW, Calgary, AB, Canada, T3E6K6
[b] Department of Earth, Energy, and Environment, University of Calgary, 2500 University Drive NW, Calgary, AB, Canada, T2N1N4
[c] Department of Geosciences, Colorado State University, 1482 Campus Delivery, Fort Collins, CO, USA, 80523-1482
[d] Department of Geosciences, Virginia Tech, 926 West Campus Drive, Blacksburg, VA, USA, 24061

ARTICLE INFO

Keywords:
Submarine channels
Stratigraphic architecture
Turbidites
Deep-water sedimentary processes
Subsurface reservoirs
Sandstone proportion

ABSTRACT

Lithologic variations in deep-water slope channel systems provide critical insight into sedimentary processes on deep-water slopes, and are a key control on natural resource distribution and connectivity in subsurface reservoirs associated with ancient deep-water systems. While many studies have described these variations at outcrop-scale along depositional strike (across-channel), few have focused on documenting along-depositional-dip changes due to: (1) the dearth of along-slope perspectives afforded by outcrops; or (2) limited resolution and coverage of subsurface data sets. In this study, slope channel elements ($\leq$30 m thick; $\leq$400 m wide) and composite channelform bodies composed of $\geq$2 stacked channel elements (channel complexes and channel systems; >30 m thick; >400 m wide) were characterized along a 50-km-long depositional-dip-oriented outcrop belt of the Campanian-Maastrichtian Tres Pasos Formation (Chile) to constrain longitudinal changes in channel fill character and stacking patterns. Results show that channel elements become more sandstone-rich downdip. Outcrop observations are supported by channel element net-to-gross ratios (measures of sandstone proportion), which increase downdip. Sandstone-prone channel elements within channel complexes and channel systems are more prevalent downdip; however, variability in lateral and vertical offset between successive channel elements downdip results in a poor correlation between net-to-gross values and paleoslope position when composite channelform bodies are considered. These findings suggest that the along-slope distribution of coarse-grained sediment in channel systems is tied to the degree of coarse-grained sediment bypass and erosion that occurs along a slope. The results of this study provide a detailed perspective into downdip changes in slope channel fill and stacking patterns, and help clarify aspects of analogous subsurface reservoirs, including sandstone proportion trends for several scales of deep-water slope channel architecture.

1. Introduction

Deep-water slope channel systems transfer sediment in some of the most remote environments on Earth (e.g., Symons et al., 2016; Azpiroz-Zabala et al., 2017). While the nature and breadth of sedimentary processes that occur in these settings has been explored in detail through recent seafloor studies and flume experiments (e.g., Straub et al., 2011; Xu et al., 2013; Cartigny et al., 2014; Hughes Clarke, 2016; Steel et al., 2017; Englert et al., 2021; Heijnen et al., 2022), understanding the relationship between sedimentary processes in deep-water slope channel systems and the development of lithologic and architectural variations in the stratigraphic record remains a topic of current research (e.g., Hage et al., 2018; Vendettuoli et al., 2019; Englert et al., 2020, 2021; Reguzzi et al., 2023). Many workers have examined ancient deep-water channel systems to better constrain process-product relationships using outcrops (e.g., Beaubouef et al., 1999; Flint et al., 2011; Englert et al., 2018; Nesbit et al., 2021; Bozetti et al., 2023), core and wireline logs (e.g., Samuel et al., 2003; Jackett et al., 2014), and seismic-reflection surveys (e.g., Abreu et al., 2003; Janocko et al., 2013; Ma et al., 2020). These studies have provided the basis for numerous facies models (e.g., Clark and Pickering, 1996; Sullivan et al., 2000; Macauley and Hubbard, 2013), which emphasize the role of sedimentary processes in the evolution of slope deposit architecture (e.g., McHargue et al., 2011; Hubbard et al., 2020).

* Corresponding author. Department of Earth and Environmental Sciences, Mount Royal University, 4825 Mount Royal Gate SW, Calgary, AB, Canada, T3E6K6.
E-mail address: bdaniels@mtroyal.ca (B.G. Daniels).

https://doi.org/10.1016/j.marpetgeo.2024.106869
Received 20 December 2023; Received in revised form 8 April 2024; Accepted 22 April 2024
Available online 24 April 2024

To date, studies of facies relationships, architectural element geometry, and stacking patterns in ancient deep-water slope channel systems have principally focused on along-depositional-strike (across-channel) perspectives of channel systems, which are afforded by most outcrops (e.g., Arnott, 2007; Pyles et al., 2010; Çelik and Cronin, 2020), and can be readily extracted from some subsurface data sets (e.g., seismic cross-sections; e.g., Deptuck et al., 2003). Though the topic of downslope changes in channel fill and architecture has been discussed previously (e.g., Plink-Björklund et al., 2001; Gardner et al., 2003; Saller and Dharmasamadhi, 2012; Bell et al., 2020), studies of down-depositional-dip (down-channel) changes in slope channel fill and stratigraphic stacking are few in number (e.g., Kneller et al., 2020; Tek et al., 2020). Characterization of longitudinal trends in channel fill and architecture using deposits from ancient systems has proven challenging in many cases, owing to: (1) the paucity of downslope perspectives afforded by most outcrops (e.g., Li et al., 2016; Englert et al., 2018); (2) the restricted spatial distribution of cores or wireline logs from wells that penetrate slope channel deposits in the subsurface (e.g., Jobe et al., 2011; Zhang et al., 2018); and (3) the nature and limited resolution of seismic data sets, which typically cannot resolve bed- to bedset-scale

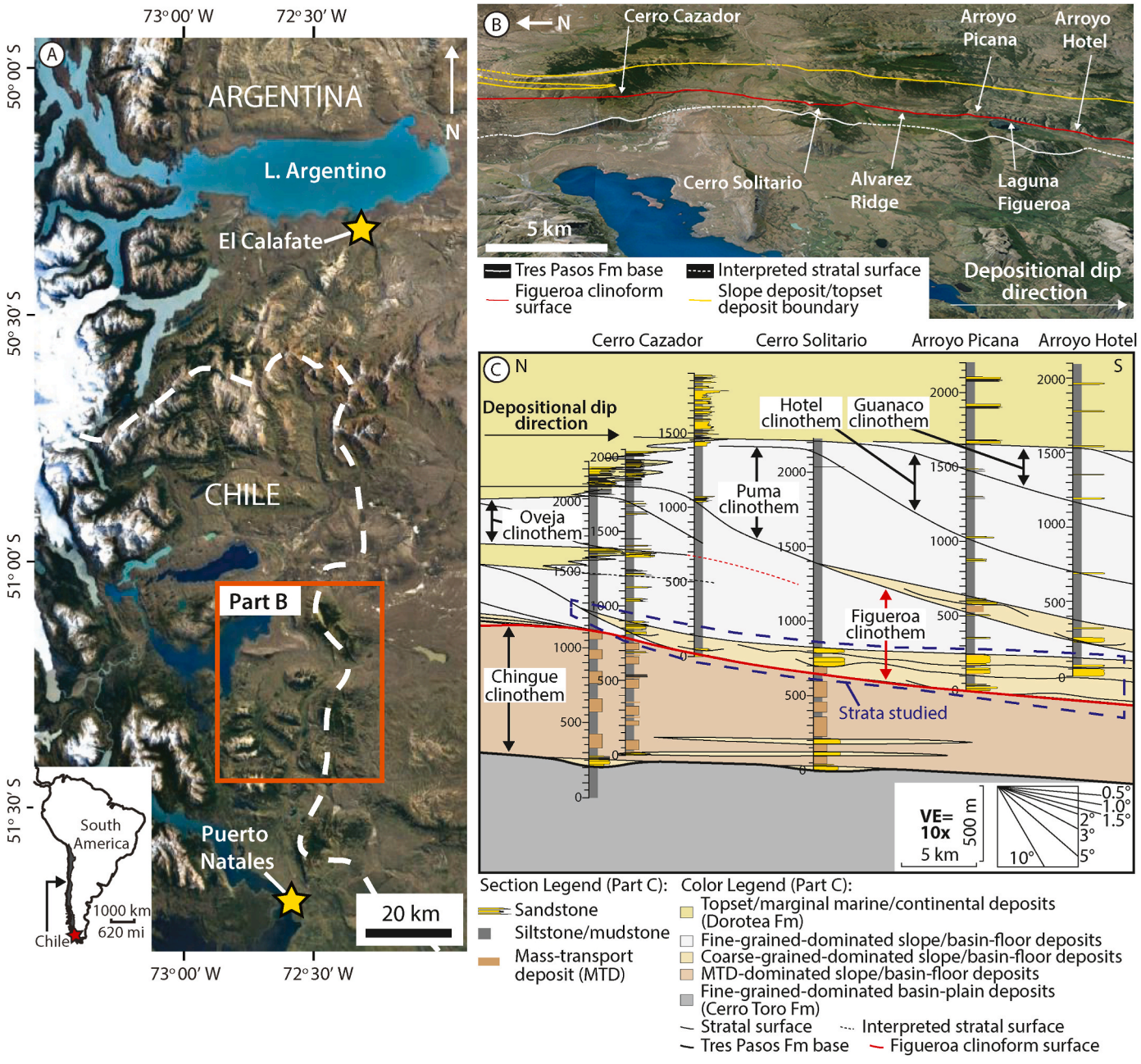

Fig. 1. Location of the study area and summary of key geologic features associated with the Tres Pasos Formation. (A) Overview of present day geography of Chilean and Argentine Patagonia in the vicinity of the study area (image data: Google, Landsat, Copernicus, 2016, http://www.google.com/earth/index.html, center of image coordinates: 50°54′09.16″S, 72°32′08.26″W). The location of this region in the context of South America is indicated on the inset map. (B) Perspective image of the study area, looking down tectonic dip to the east (image data: Google, Centre National d'Études Spatiales, Astrium, Landsat, Copernicus, 2016, http://www.google.com/earth/index.html, center of image coordinates: 51°15′55.44″S, 72°31′13.12″W). Key geographic features referenced in this study area are indicated; the base of the stratigraphic interval of interest is demarcated with a red line. (C) Stratigraphic cross-section of the strata exposed along the outcrops shown in (B). The extent of the Figueroa clinothem, which is the interval of interest for this study, is indicated with red arrows. Within the Figueroa clinothem, slope channel deposit-prone strata have been indicated with blue dashed lines. Modified from Daniels et al. (2018) and Bauer et al. (2020).

characteristics of individual channel fills (e.g., channel elements; Bakke et al., 2011; Pemberton et al., 2018). Documenting downslope changes in slope channel fill and architecture is critical for constraining the range and relative importance of sediment transfer processes along slopes (e.g., bypass, erosion, deposition), and can aid with the characterization of subsurface reservoirs associated with ancient deep-water slope systems worldwide (e.g., Posamentier and Kolla, 2003; Mayall et al., 2006; Morris et al., 2014).

In this study, Campanian slope channel deposits of the Tres Pasos Formation of southern Chile are examined (Fig. 1). Outcrops of the Tres Pasos Formation feature near-continuous exposures of slope channel systems that can be correlated for up to ~50 km along-depositional-dip (Hubbard et al., 2010; Daniels et al., 2018; Bauer et al., 2020). The analysis emphasizes characterization of channel elements (≤30 m thick, ≤400 m wide), as well as composite channelform bodies that are composed of ≥2 stacked channel elements (i.e., channel complexes and channel systems; >30 m thick; >400 m wide). Outcrop results were considered alongside core, wireline log, and 2-D seismic data from other high-relief slope systems documented in the subsurface (Porter et al., 2006; Deptuck et al., 2007; Cross et al., 2009; Morris et al., 2014; Fowler and Novakovic, 2018; Sansom, 2018). The primary objective of the study is to characterize the downdip facies and stacking pattern variability of slope channel stratigraphy. Results are used to inform how the record of fundamental sediment transfer processes are variably preserved longitudinally, with an emphasis on sandstone distribution.

2. Geologic history of the Tres Pasos Formation, southern Chile

Deposits of the Tres Pasos Formation preserve a Campanian-Maastrichtian archive of tectonic and sedimentary processes in the Magallanes-Austral retroarc foreland basin of Chilean Patagonia (Fig. 1; Katz, 1963; Macellari et al., 1989; Romans et al., 2011). The development of deep-water environments in the basin is related to the pre-Cretaceous history of the region, where rifting and extension linked to the breakup of Gondwana led to the formation of the Rocas Verdes backarc basin (Dalziel et al., 1974; de Wit and Stern, 1981; Fildani and Hessler, 2005). During the Aptian, increased spreading rates in the South Atlantic Ocean and elevated convergence rates on the western margin of South America initiated the closure of the Rocas Verdes backarc basin (Calderón et al., 2016; Malkowski et al., 2017). Increased Andean uplift, coupled with the loading of attenuated crust inherited from the extensional phase, promoted high amplitude and short wavelength basin subsidence and led to the formation of the Magallanes-Austral retroarc foreland basin (Fosdick et al., 2014). Underfilled deep-water conditions persisted in the basin until the Maastrichtian (Romans et al., 2011).

The Tres Pasos Formation is a 2500 m-thick interval of deep-water siltstone and sandstone deposited during the Campanian-Maastrichtian (Fig. 1; Katz, 1963; Hubbard et al., 2010; Daniels et al., 2019). The interval overlies deep-water units of the Coniacian-Campanian Cerro Toro Formation, and is overlain by marginal marine and terrestrial deposits of the Campanian-Maastrichtian Dorotea Formation (Fig. 1; Smith, 1977; Hubbard et al., 2008; Covault et al., 2009; Schwartz and Graham, 2015; Bozetti et al., 2023). Deposits of the Tres Pasos Formation can be traced up-depositional-dip into coeval units of the Dorotea Formation (Fig. 1; Bauer et al., 2020); together, these formations record the progressive infilling of the Magallanes-Austral Basin towards the end of the Cretaceous (Daniels et al., 2018).

This study is focused on outcrops of the Tres Pasos Formation exposed north of Puerto Natales, Chile (Fig. 1). In this area, the formation has been subdivided into five distinct stratigraphic packages bounded by regionally extensive stratigraphic surfaces that dip slightly southward relative to the regional eastward-dipping structure (Fig. 1; Hubbard et al., 2010). These packages represent southward-prograding shelf margin clinothems (Hubbard et al., 2010). In some instances, bounding clinoform surfaces are overlain by thick, sandstone-rich deposits that record periods of prolonged off-shelf transfer of coarse-grained sediment (Bauer et al., 2020). The Figueroa clinothem is associated with a slope with >1000 m of relief that was >40 km long, and is the focus of this analysis (Fig. 1).

3. Architectural element hierarchy

Slope channel stratigraphy is commonly characterized by multiple scales of channelform bodies, which has promoted hierarchical classification of deposits to inform the long-term evolution of slope systems (see Cullis et al., 2018 for a comprehensive overview of different hierarchical classifications for deep-water slope channel deposits). While hierarchical frameworks have mainly been applied to assist with understanding predictability, heterogeneity, connectivity, and performance in deep-water slope reservoirs (e.g., Clark and Pickering, 1996; Alpak et al., 2013; Jackson et al., 2019), they are also used to provide insight into the nature of sedimentary processes on deep-water slopes (e.g., Mutti and Normark, 1987; Di Celma et al., 2011; Bain and Hubbard, 2016).

A channel element is a mappable body that is interpreted to record erosional and/or depositional processes involved in the sculpting and filling of a single geomorphic feature on the seafloor (Fig. 2; Mutti and Normark, 1987; Hubbard et al., 2014, 2020). For this study, analysis of slope deposits utilized a threefold hierarchical framework that distinguishes channel elements from larger, more composite features (Fig. 2; *sensu* Sprague et al., 2002, 2005; McHargue et al., 2011). The next largest hierarchical order discussed is a "complex" (Sprague et al., 2002, 2005; McHargue et al., 2011; Pyles et al., 2014), which consists of ≥2 elements that stack in a consistent pattern (Fig. 2). Complex boundaries are marked by abrupt changes in lateral and/or vertical offset between successive elements (McHargue et al., 2011). A collection of ≥2 complexes represents the largest hierarchical order evaluated, and are commonly referred to as "complex sets" (Sprague et al., 2002, 2005; McHargue et al., 2011). Herein, we use the term "channel system" to describe all stratigraphic intervals that contain ≥2 complexes (Fig. 2).

4. Data and methods

4.1. Field data collection and stratigraphic mapping

Outcropping Tres Pasos Formation deposits were characterized using stratigraphic sections (247 sections; total thickness: 10162 m), which capture bed thickness and grain size trends, as well as sedimentary structures and bedding geometries. Deposits described in measured section were correlated along the outcrop belt using differential GPS mapping of key stratigraphic surfaces (e.g., erosion surfaces at channel element bases), paleocurrent data, and integration of ground- and uncrewed-aerial-vehicle-based photography with satellite imagery. Stratigraphic correlation efforts also employed a point projection workflow optimized for Petrel software (Schlumberger, 2014). This workflow involves projection of GPS points according to the bedding orientation onto a two-dimensional plane that is perpendicular to bedding (striking north-south, dipping west), which enables visualization of outcropping bodies in space where structural tilt has been removed (cf. Englert et al., 2018). All mapping and point projection results are the foundation of stratigraphic cross-sections and slope deposit stacking pattern diagrams at all outcrop locations.

4.2. Comparisons to ancient deep-water slope systems in the subsurface

Results from the Tres Pasos Formation were compared with data from other high-relief (i.e., >500 m shelf-to-basin relief) slope systems documented in the subsurface. Comparison of channel elements and channel complexes documented in outcrop and subsurface data sets was performed via analysis of net-to-gross ratios computed from vertical stratigraphic sections (Tres Pasos Formation), as well as from core

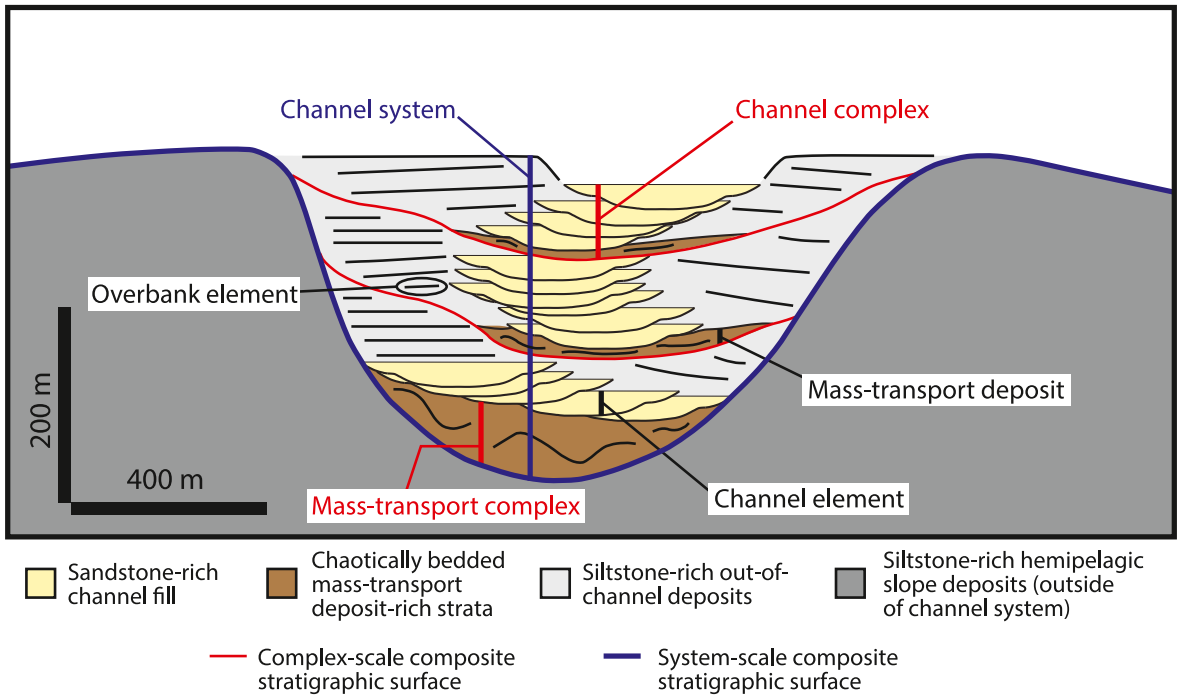

Fig. 2. Schematic representation of architectural elements discussed in this study. Fundamental architectural elements are indicated with black text, while complex- and system-scale composite architectural elements are indicated with red and blue text respectively.

descriptions and/or wireline logs (subsurface data sets; Porter et al., 2006; Cross et al., 2009; Morris et al., 2014; Fowler and Novakovic, 2018; Sansom, 2018). For analyses of channel elements and channel complexes, net-to-gross ratios are computed from the total thickness of all coarse-grained units (i.e., sandstone) in a stratigraphic interval divided by the gross thickness of that interval (see Appendix A and Appendix B for details on net-to-gross calculations). Channel element and channel complex boundaries identified in measured sections and logs were used to constrain gross interval thicknesses and enable hierarchy-specific net-to-gross calculations.

Comparison at the scale of channel systems focused on an analysis of net-to-gross values from the Tres Pasos Formation and a Pleistocene channel system from the subsurface offshore of Nigeria (i.e., the Benin-major channel system; Deptuck et al., 2007, Fig. 3). Because continuous vertical sections through outcrop and subsurface datasets are rare, an alternate method for calculating net-to-gross ratios was required. High-resolution constraints on the boundaries of the Benin-major system are evident in seismic data (seismic frequency: >65 Hz; Fig. 3A; Appendix C), and 15 vertical lines were equally spaced between the lateral boundaries of the system in each cross-section. These vertical lines extend to the base of the channel system, which is defined by a prominent concave-upward high-amplitude reflection (Fig. 3A; Deptuck et al., 2007). The top is demarcated by a laterally extensive, high-amplitude sub-horizontal reflection, which represents the modern seafloor (Fig. 3A; Deptuck et al., 2007). Within channel system strata, intervals with high-amplitude concave-upward reflections (channel fills) were assigned an 85% net-to-gross ratio (Fig. 3A). This 85% net-to-gross ratio is the average net-to-gross ratio computed from all channel element intervals examined in this study (number of intervals examined = 399; see Appendix A for raw data), and it has been applied to intervals with high-amplitude concave-upward reflections to capture the apparent sandstone-rich nature of the Benin-major channel fills (Deptuck et al., 2007). Concave-upward reflections are commonly found adjacent to intervals with low-amplitude sub-horizontal reflections. These intervals are interpreted to reflect siltstone-rich out-of-channel deposits (Deptuck et al., 2007), which may be associated with overbank settings (submarine levees, terraces). Overbank settings can possess net-to-gross ratios that are less than 10% in cases where mudstone-rich successions are documented and more than 20% in cases where successions with more abundant sandstone beds are documented (Mayall and Kneller, 2021). In light of this information, we assigned a net-to-gross value of 15% (the average of the aforementioned quoted net-to-gross values) to all intervals that contain low-amplitude sub-horizontal reflections (Fig. 3A). Intervals of chaotic seismic facies are also observed in seismic cross-sections of the Benin-major system (Fig. 3A). These intervals largely record submarine mass-wasting processes (Deptuck et al., 2007). Since these intervals are thought to be linked to remobilization of siltstone/mudstone-rich out-of-channel deposits in the Benin-major system (Deptuck et al., 2007), we have assigned a 15% net-to-gross ratio to these intervals as well (Fig. 3A). While these assumptions undoubtedly mask the true net-to-gross variability within each of the aforementioned seismic stratigraphic intervals, we apply them here to obtain a first-order, data-driven estimation of net-to-gross variability in the absence of detailed vertical stratigraphic sections at the channel system scale that can be generally considered alongside results from the other hierarchical scales previously discussed.

In the outcrop belt, channel system edges are typically not readily identifiable due to vegetative cover of thick sequences of fine-grained strata. Following the technique adapted from subsurface analysis, calculation of Tres Pasos Formation channel system net-to-gross values relied on stacking pattern diagrams. Since the maximum thickness of a given channel system is well-constrained at each outcrop location, an estimate of channel system width was determined through a survey of channel system width-to-thickness ratios (W:T) from a global dataset (Fig. 3B). Channel systems considered as a part of this analysis commonly have a W:T between 10 and 20, with an average W:T of 15 (Fig. 3B). We use this average W:T to estimate the width of a given channel system along dip in the outcrop belt, as it represents a measure of central tendency for W:T that is derived from a global dataset of high-relief slope channel systems. Once the width of a channel system is established, 15 vertical lines were drawn through each channel system documented in a stacking pattern diagram (Fig. 3C). These lines formed the basis for a near-identical analysis to that employed for the subsurface dataset, where a simplified 85% net-to-gross ratio was applied to the

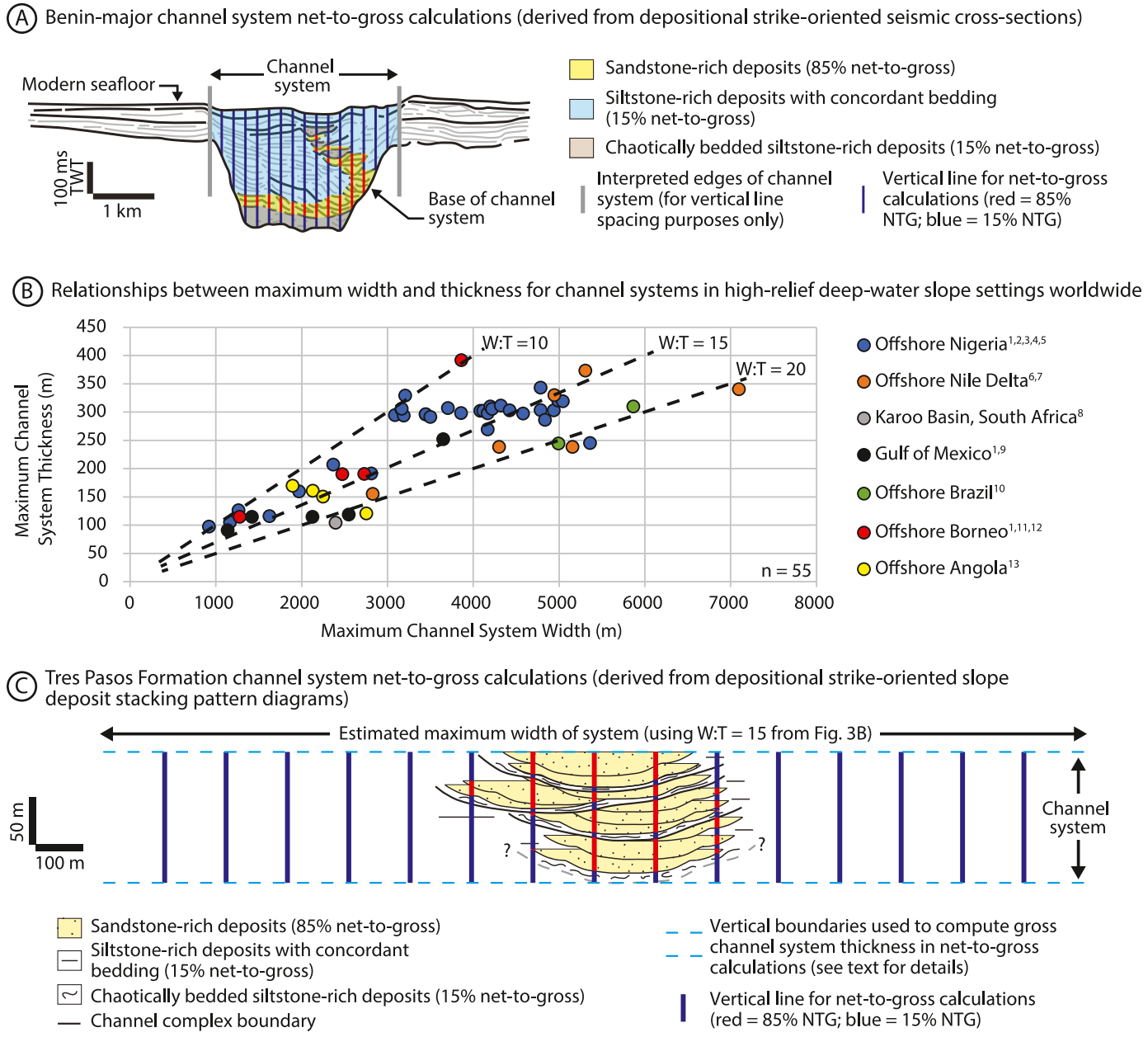

Fig. 3. (A) Visual representation of the methodology used to compute net-to-gross ratios for the Benin-major channel system. Trace diagram has been modified from Deptuck et al. (2007); trace diagrams employ the interpretations of Deptuck et al. (2007), and are based on seismic images from the Benin-major system that are presented in that study. In all trace diagrams, high-amplitude reflections are indicated with thick black lines, while low-amplitude reflections are indicated with thinner gray lines. NTG—Net-to-gross; TWT—Two-way time. (B) Scatterplot showing the range of maximum width and thickness values for a range of channel systems documented in the subsurface and outcrop from high-relief slope systems worldwide. In general, width-to-thickness ratios (W:T) plot between 10 and 20 (average = 15). Data on this plot has been derived from the following sources (indicated with superscripts in the legend): (1) Posamentier and Kolla (2003); (2) Deptuck et al. (2007); (3) Armitage et al. (2012); (4) Janocko et al. (2013); (5) Jobe et al. (2015); (6) Catterall et al. (2010); (7) Morris et al. (2014); (8) Hodgson et al. (2011); (9) Sylvester et al. (2012); (10) Qin et al. (2016); (11) Saller et al. (2010); (12) Saller and Dharmasamadhi (2012); and (13) Mayall et al. (2006). Raw data associated with channel system measurements featured in this plot are provided in Appendix A. (C) Visual representation of the methodology used to compute net-to-gross ratios for the Tres Pasos Formation channel systems. The dashed gray line present near the bottom of the stacking pattern diagram represents the base of an interval of chaotically bedded strata; the lowest point along this line is interpreted to closely coincide with the position of the master bounding surface associated with a given channel system. Since the exact geometry and full extent of this bounding surface is not able to be constrained using available outcrop exposure, along-strike net-to-gross calculations employ the maximum documented channel system thickness (indicated with blue dashed lines) in all cases.

sandstone-rich areas of channel elements as presented in each stacking pattern diagram (Fig. 3C), and a 15% net-to-gross ratio was assigned to all siltstone-rich or mass-transport-deposit-rich areas (Fig. 3C).

5. Outcrop mapping results

5.1. Lithofacies and lithofacies associations

Tres Pasos Formation deposits were grouped into eight lithofacies (LF) to characterize the record of sedimentary processes along the paleoslope (Fig. 4). Lithofacies include: (1) thick-bedded pebbly

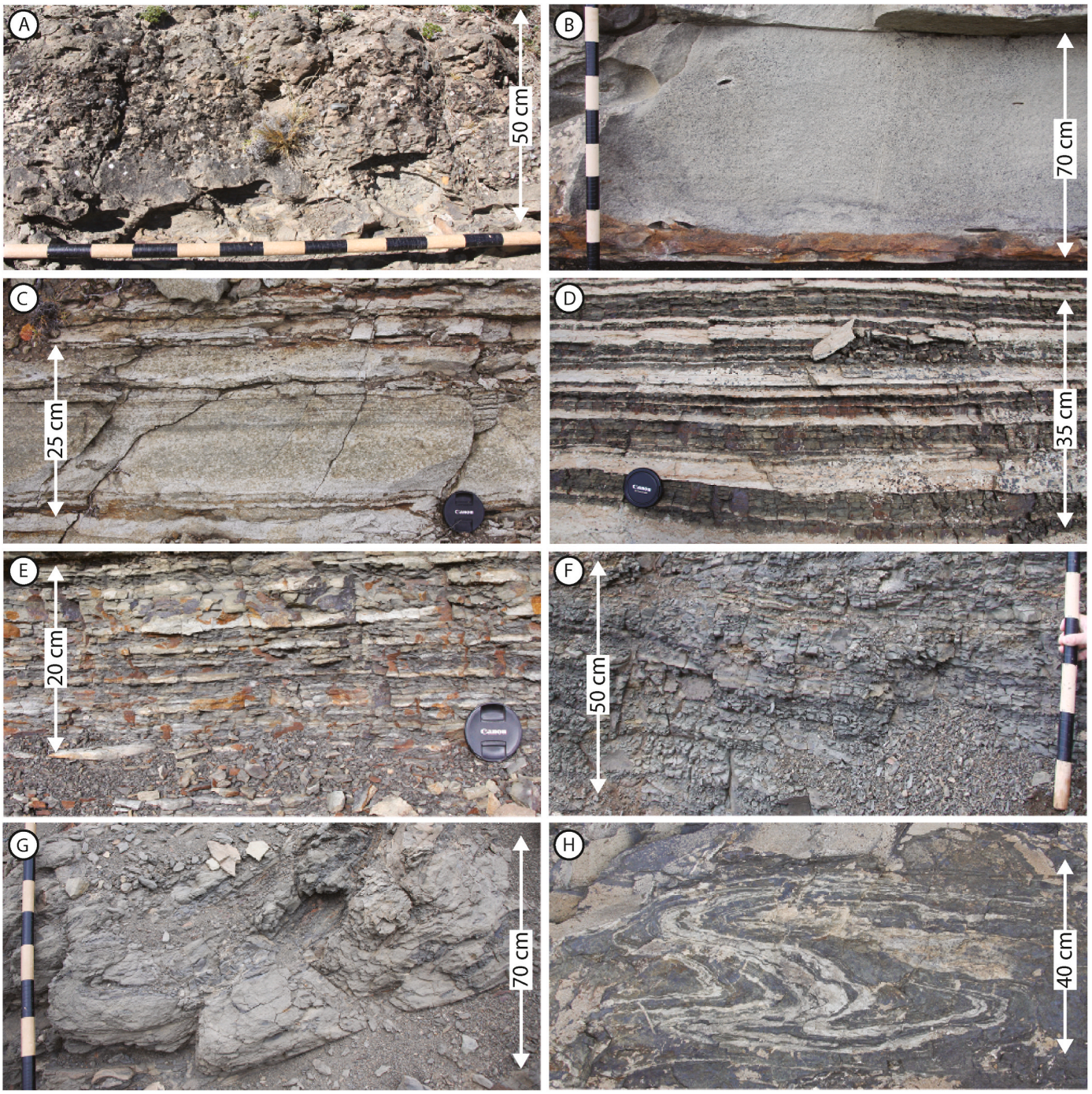

Fig. 4. Lithofacies of studied strata within the Tres Pasos Formation. (A) LF1 – Thick-bedded pebbly sandstone; (B) LF2 – Thick-bedded sandstone; (C) LF3 – Medium-bedded sandstone; (D) LF4 – Thin-bedded sandstone and siltstone; (E) LF5 – Siltstone with very-thin-bedded sandstone; (F) LF6 – Structureless siltstone; (G) LF7 – Disorganized sandy to gravelly mudstone; (H) LF8 – Mudstone with disorganized and/or disturbed sandstone beds. Jacob's staff (Parts A-B, F-G) is marked with 10 cm increments. Camera lens cap (Parts C-E) is 5.8 cm in diameter. A summary of all lithofacies characteristics is provided in Table 1.

sandstone (LF1; Fig. 4A); (2) thick-bedded sandstone (LF2; Fig. 4B); (3) medium-bedded sandstone (LF3; Fig. 4C); (4) thin-bedded sandstone and siltstone (LF4; Fig. 4D); (5) siltstone with very-thin-bedded sandstone (LF5; Fig. 4E); (6) structureless siltstone (LF6; Fig. 4F); (7) disorganized sandy to gravelly mudstone (LF7; Fig. 4G); and (8) mudstone with disorganized and/or disturbed sandstone beds (LF8; Fig. 4H). Lithofacies descriptions and interpretations are summarized in Table 1. Lithofacies reflect the products of high- and low-density turbidity currents, as well as submarine mass-wasting processes (Bouma, 1962; Middleton and Hampton, 1976; Lowe, 1982; Talling et al., 2012).

Observations of lithofacies arrangement patterns in outcrop led to definition of six lithofacies associations (LFA). Lithofacies associations include: (1) thick-bedded, amalgamated sandstone-rich deposits (LFA1; Fig. 5A); (2) medium-to thick-bedded, non-amalgamated sandstone-rich deposits (LFA2; Fig. 5B); (3) sandstone-rich interbedded sandstone and siltstone (LFA3; Fig. 5C); (4) siltstone-rich interbedded sandstone and siltstone with discontinuous sandstone beds and laminations (LFA4; Fig. 5D); (5) siltstone-dominated deposits (LFA5; Fig. 5E); and (6) disorganized and/or chaotically bedded deposits (LFA6; Fig. 5F). Lithofacies association descriptions and interpretations are listed in Table 2.

Table 1
Summary of lithofacies of the Figueroa clinothem (Tres Pasos Formation).

Lithofacies	Lithology description	Grading	Bed and facies thickness	Basal bounding surface	Key sedimentary features and lithologic accessories	Overall bioturbation	Interpreted sediment transfer processes	References
LF1: Thick-bedded pebbly sandstone (Fig. 4A)	Pebbly sandstone, medium- to very coarse-grained sandstone matrix	Normal grading	Beds: 0.5–4.0 m Facies: up to 10.0 m	Sharp to undulating, commonly amalgamated, commonly erosive	Massive beds (Ta/S3), abundant extrabasinal pebbles and/or elongated mudstone intraclasts along basal bounding surfaces (common a-axis measurement range: 0.01–0.12 m)	None	High-density turbidity current (or concentrated density flow); deposition following traction and turbulent suspension of sediment; elevated erosion and scouring	Bouma (1962); Lowe (1982); Mutti and Normark (1987, 1991); Fildani et al. (2013); Hubbard et al. (2014)
LF2: Thick-bedded sandstone (Fig. 4B)	Fine- to very coarse-grained sandstone (very coarse-grained units are commonly found towards the base of the lithofacies)	Normal grading	Beds: 0.5–6.0 m Facies: up to 14.0 m	Sharp to undulating, amalgamated or non-amalgamated, commonly erosive	Incomplete Bouma/Lowe sequences (Ta/S3 to Tc), mudstone intraclasts commonly found along basal bounding surfaces (common a-axis measurement range: 0.01–0.05 m)	None to very low	High- to low-density turbidity current; deposition following traction and turbulent suspension of sediment; reduced erosion and scouring compared to LF1	Bouma (1962); Lowe (1982); Mutti and Normark (1987, 1991); Macauley and Hubbard (2013); Hubbard et al. (2014, 2020)
LF3: Medium-bedded sandstone (Fig. 4C)	Fine- to coarse-grained sandstone	Normal grading	Beds: 0.1–0.5 m Facies: up to 10.0 m	Sharp to undulating, rarely amalgamated	Incomplete Bouma sequences (dominantly Ta to Tc), matrix is organic-rich in certain instances	None to high in organic-rich intervals	Low-density turbidity currents with progressively lower concentration and velocity; deposition following traction, saltation, and suspension of sediment; reduced erosion and scouring compared to LF1 and LF2	Bouma (1962); Lowe (1982); Mutti and Normark (1987, 1991); Macauley and Hubbard (2013); Hubbard et al. (2014, 2020)
LF4: Thin-bedded sandstone and siltstone (Fig. 4D)	Very fine- to fine-grained sandstone interbedded with siltstone	Normal grading	Sandstone beds: 0.05–0.2 m Siltstone beds: up to 0.03 m Facies: up to 6.0 m	Sharp to undulating, non- amalgamated	Incomplete Bouma sequences (dominantly Tb to Td)	Low to high	Low-density turbidity currents; deposition following traction, saltation, and suspension of sediment; variable amounts of erosion and scouring	Bouma (1962); Lowe (1982); Mutti and Normark (1987, 1991); Macauley and Hubbard (2013); Hubbard et al. (2014, 2020)
LF5: Siltstone with very-thin-bedded sandstone (Fig. 4E)	Primarily siltstone with minor fine- to very-fine-grained sandstone beds and laminations	Normal grading	Sandstone beds: up to 0.05 m Siltstone beds: up to 0.5 m Facies: up to 5.0 m	Sharp	Incomplete Bouma sequences (dominantly Tc to Te)	None to very low	Low-density turbidity currents; deposition following saltation and suspension of sediment; very little erosion and scouring	Mutti and Normark (1987, 1991); Talling et al. (2012); Macauley and Hubbard (2013); Hubbard et al. (2014)
LF6: Structureless siltstone (Fig. 4F)	Siltstone	Not graded	Beds: up to 4.0 m Facies: up to 20.0 m	Sharp	Structureless beds (possibly Te)	None	Hemipelagic and dilute low-density turbidity currents; deposition following suspension	Bouma (1962); Talling et al. (2012)
LF7: Disorganized sandy to gravelly mudstone (Fig. 4G)	Sand and granules immersed in a mud-rich matrix	Not graded	Beds: no bedding observed Facies: up to 15.0 m	Sharp	Extrabasinal granules	None	Cohesive mud flows or debris flows; deposition following flow "freezing"	Hampton (1972); Middleton and Hampton (1973, 1976); Talling et al. (2012)
LF8: Mudstone with disorganized and/or disturbed sandstone beds (Fig. 4H)	Mudstone, siltstone, and fine-grained sandstone	Normal grading in contorted sandstones	Beds: highly variable (beds are deformed) Facies: up to 10.0 m	Sharp	Chaotic and/or contorted bedding	None	Deposition following mass-wasting (i.e., slumping) caused by depositional overloading or gravity induced sliding	Hampton (1972); Middleton and Hampton (1973, 1976); Talling et al. (2012)

Lithofacies associations are interpreted to record distinct subenvironments in deep-water slope systems, including channelized settings (LFA1-4; e.g., Hubbard et al., 2014), overbank settings (LFA5; e.g., Kane and Hodgson, 2011), and mass-transport-dominated settings (LFA6; e.g., Armitage et al., 2009).

5.2. Fundamental architectural elements

Analysis of lithofacies associations and stratigraphic architecture informed characterization of fundamental architectural elements along the outcrop belt (Fig. 1). These elements include: (1) channel elements, which were subdivided into two different types (Type 1 and Type 2; Fig. 6); (2) overbank elements (Fig. 7); and (3) mass-transport deposits (Fig. 7).

5.2.1. Type 1 channel elements

Description: Type 1 channel elements are 10–30 m thick and 150–400 m wide in depositional strike cross-section (Fig. 6). The basal surfaces of these features have a concave-upward channelform shape, and truncate underlying strata. An up to 10 m thick interval of amalgamated sandstone-rich deposits (LFA1-rich units) typically overlies the basal surface in the axes of these bodies (Fig. 5A); this interval can contain abundant extrabasinal pebbles and mudstone intraclasts (Fig. 6D). Sandstone-rich intervals also contain concave-upward surfaces that roughly mimic basal channelform surfaces. These surfaces variably truncate adjacent units and exhibit 3–6 m of relief (Fig. 6). Sandstone-rich intervals are overlain by packages of siltstone-rich interbedded units with discontinuous sandstone beds (LFA4; Fig. 5D and 6). Stratal surfaces within siltstone-rich intervals could not be resolved due to the recessive nature of associated outcrop exposures (Fig. 6D). Top surfaces of Type 1 channel elements are flat (Fig. 6). Type 1 channel elements are only seen in the northern portion of the outcrop belt (i.e., Cerro Cazador to Alvarez Ridge; Fig. 1).

Interpretation: Type 1 channel elements record erosion, sediment bypass, and deposition within slope channels (Mutti and Normark, 1987; Gardner et al., 2003; Hubbard et al., 2014, 2020). Truncation along basal surfaces records erosion during channel establishment (Fildani et al., 2013). Lateral and vertical lithofacies association trends suggest relatively high energy in channel axes and lower energy towards channel margins (Mutti and Normark, 1991). Truncation along concave-upward surfaces within channel elements records multiple phases of cut and fill during channel element evolution (Hubbard et al., 2014, 2020). The limited amount of coarse-grained detritus in these elements can be linked to turbidity currents that largely bypassed their coarse-grained load basinward (Mutti and Normark, 1987; Fildani et al., 2013). Under these circumstances, coarse-grained units near channel element bases represent a component of the flow that was not transferred further downslope (Fig. 6; Hubbard et al., 2010). Overlying siltstone-rich units record deposition from the dilute tails of bypassing turbidity currents, or channel abandonment processes (Mutti and Normark, 1987; Stevenson et al., 2015).

5.2.2. Type 2 channel elements

Description: Type 2 channel elements are 10–30 m thick and 150–400 m wide in depositional strike cross-section (Fig. 6). Basal surfaces are channelform in shape, truncate underlying strata, and are sometimes overlain by <1 m thick intervals of siltstone-rich interbedded units with discontinuous sandstone beds (LFA4; Fig. 5D). Above these intervals, Type 2 channel elements contain amalgamated sandstones (LFA1-rich units) in axial positions that transition to non-amalgamated and interbedded units (LFA2-and LFA3-rich units) towards their margins (Fig. 6). Concave-upward intra-element erosion surfaces, which often exhibit 3–6 m of relief, are common. Top surfaces of Type 2 channel elements are often flat (Fig. 6); however, due to the stacked nature of channel elements, top surfaces are typically truncated by successive channel element erosion surfaces. Type 2 channel elements are observed at all outcrop locations.

Interpretation: Type 2 channel elements also record erosion, sediment bypass, and deposition within slope channels (Hubbard et al., 2014, 2020); however, lithofacies association distributions suggest that the evolutionary history of these channel elements is different compared to Type 1 channel elements. Basal incision surfaces record erosion during channel establishment (Fildani et al., 2013); fine-grained lithofacies associations that directly overlie basal surfaces record deposition from the tails of turbidity currents that largely bypassed coarse-grained material downslope (Stevenson et al., 2015). Axis to margin lithofacies association transitions in the overlying units reflect higher-energy sediment transfer in channel axes, and lower-energy sediment transfer near channel margins (Macauley and Hubbard, 2013). Intra-element erosion surfaces record multiple phases of cut and fill during channel element evolution (Hubbard et al., 2014, 2020). The prevalence of coarse-grained detritus within these channel elements reflects increased coarse-grained sediment deposition during channel filling (Mutti and Normark, 1987; Gardner et al., 2003).

5.2.3. Overbank elements

Description: Overbank elements, which occur lateral to and stratigraphically above channel elements, are up to 25 m thick and are at least 100s of m wide where exposed (Fig. 7A). Basal surfaces are flat and rarely display evidence for truncation of nearby units. Overbank elements are mainly composed of siltstone-rich deposits (LFA5; Fig. 5E and 7A); however, thicker sandstone beds are sometimes present (Fig. 7A). Notable lithofacies changes include: (1) lateral transitions from LF5-rich strata to LF6-rich strata with increasing distance away from channel elements (i.e., fining away from channel elements); and (2) vertical transitions from LF5-rich strata to LF6-rich strata (i.e., 5–10 m thick fining-upward packages; Fig. 5E). Top surfaces of overbank elements are flat. Overbank elements are observed at all outcrop locations.

Interpretation: Overbank elements reflect deposition from low-density turbidity currents in non-channelized areas (e.g., Pirmez and Flood, 1995; Hansen et al., 2015). The lack of truncation along basal surfaces suggests limited erosion during their formation. Lithofacies trends suggest waning flow energy with increasing distance away from channel elements.

Overbank elements that occur lateral to channel elements record deposition in a submarine levee or terrace setting (Kane and Hodgson, 2011; Hansen et al., 2019). This interpretation is supported by an increased proportion of siltstone-rich deposits within overbank elements with increasing distance from channel elements, which is observed in many submarine levee and terrace settings globally (Hiscott et al., 1997; Beaubouef, 2004; Kane et al., 2007). Thick sandstone beds within overbank elements found lateral to channel elements may reflect coarse-grained splays in overbank regions (Pirmez et al., 1997; Hubbard et al., 2009; Di Celma et al., 2011). Overbank elements that overlie channel elements record channel avulsion as the channel migrates further from the point of observation (McHargue et al., 2011). Similar fining upward packages have been linked to channel avulsion processes in other systems (e.g., Labourdette, 2007; Mokhtar et al., 2016).

5.2.4. Mass-transport deposits

Description: Mass-transport deposits, which typically occur stratigraphically below thick packages of stacked channel elements and overbank elements, are up to 15 m thick and are at least 100s of m wide where exposed (Fig. 7). The basal surfaces of these deposits display irregular geometry that is linked to truncation of underlying strata. These bodies primarily contain chaotically bedded intervals (LFA6; Fig. 5F) that are sometimes overlain by thin packages of discontinuous sandstone (Appendix B, Fig. B6). Top surfaces of these elements show irregular geometry. Mass-transport deposits are observed at all outcrop locations.

Interpretation: Mass-transport deposits reflect deposition from submarine mass-wasting (e.g., a slump; Moscardelli et al., 2006; Pyles et al.,

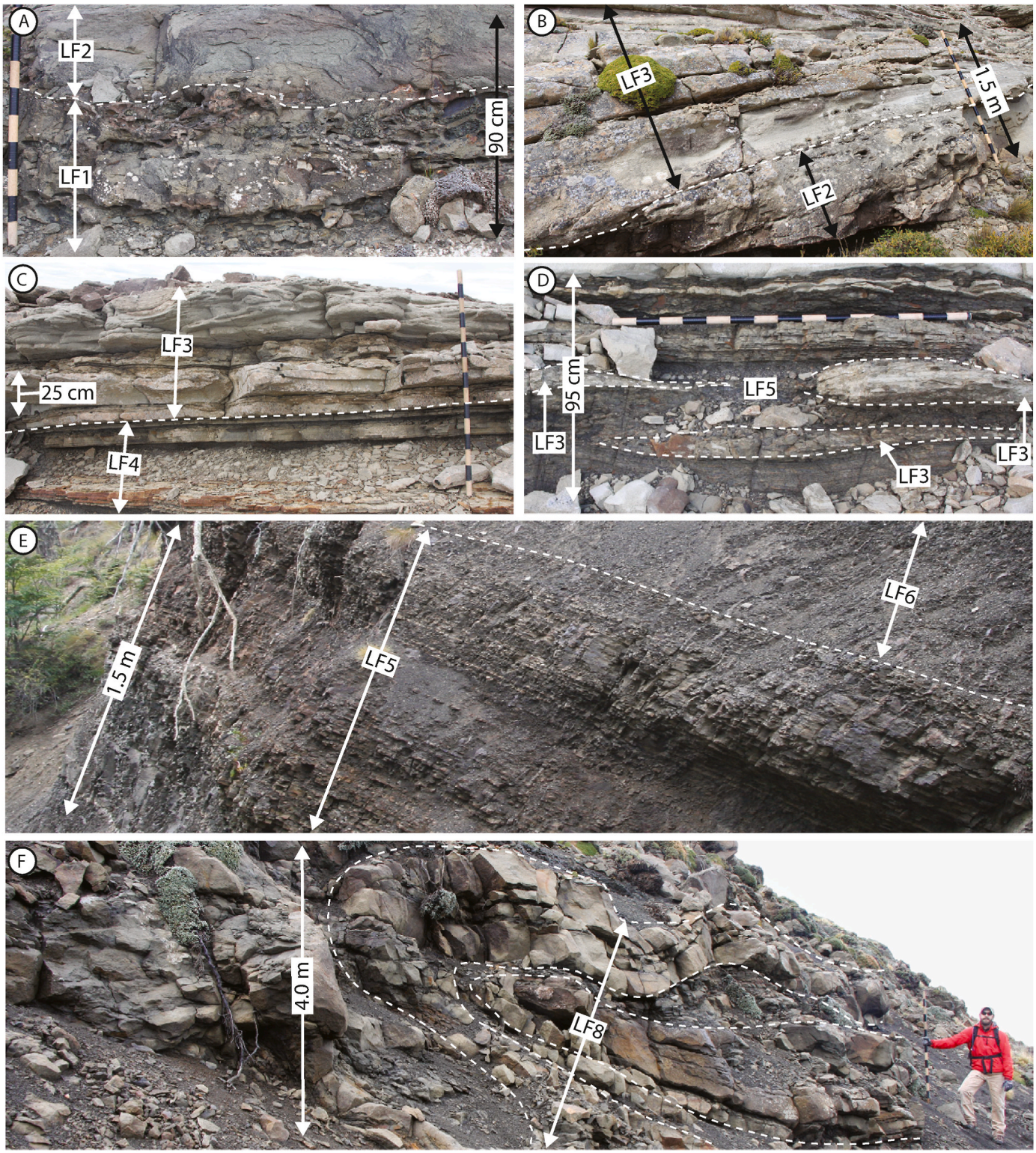

Fig. 5. Lithofacies associations of studied strata within the Tres Pasos Formation. (A) LFA1 – Thick-bedded, amalgamated sandstone-rich deposits; (B) LFA2 – Medium- to thick-bedded, non-amalgamated sandstone-rich deposits; (C) LFA3 – Sandstone-rich interbedded sandstone and siltstone; (D) LFA4 – Siltstone-rich interbedded sandstone and siltstone with discontinuous sandstone beds and laminations; (E) LFA5 – Siltstone-dominated deposits; (F) LFA6 – Disorganized and/or chaotically bedded deposits. For Parts A-E, dashed white lines indicate the boundaries of key lithofacies that make up each facies association. For Part F, dashed white lines indicate the boundaries of contorted beds. Jacob's staff (Parts A-D, F) is marked with 10 cm increments (total length = 1.5 m). A summary of all lithofacies association characteristics is provided in Table 2.

Table 2
Summary of lithofacies associations of the Figueroa clinothem (Tres Pasos Formation).

Lithofacies association	Recognized primary and secondary lithofacies	Interval thickness	Interpreted sub-environment of deposition	Architectural element association	Systematic spatial relationships with other lithofacies associations within architectural elements	References
LFA1: Thick-bedded, amalgamated sandstone-rich deposits (Fig. 5A)	Primary: LF2 Secondary: LF1	Up to 30.0 m	Axis regions of slope channels	Type 1 and Type 2 channel elements	Underlies LFA4 in Type 1 channel elements; sometimes overlies LFA4 in Type 2 channel elements; lateral transition to LFA2 towards Type 2 channel element margins	Mutti and Normark (1987, 1991); Clark and Pickering (1996); Beaubouef et al. (1999); McHargue et al. (2011); Fildani et al. (2013); Macauley and Hubbard (2013); Hubbard et al. (2014)
LFA2: Medium- to thick-bedded, non-amalgamated sandstone-rich deposits (Fig. 5B)	Primary: LF3 Secondary: LF2	Up to 25.0 m	Off-axis regions of slope channels	Type 2 channel elements	Lateral transition to LFA1 (towards axis of channel element) and LFA3 (towards margin of channel element); sometimes overlies LFA4	Clark and Pickering (1996); Beaubouef et al. (1999); McHargue et al. (2011); Fildani et al. (2013); Macauley and Hubbard (2013); Hubbard et al. (2014)
LFA3: Sandstone-rich interbedded sandstone and siltstone (Fig. 5C)	Primary: LF4 Secondary: LF3	Up to 20.0 m	Margin regions of slope channels	Type 2 channel elements	Lateral transition to LFA2 (towards axis of channel element); sometimes overlies LFA4	Clark and Pickering (1996); Beaubouef et al. (1999); McHargue et al. (2011); Fildani et al. (2013); Macauley and Hubbard (2013); Hubbard et al. (2014)
LFA4: Siltstone-rich interbedded sandstone and siltstone with discontinuous sandstone beds and laminations (Fig. 5D)	Primary: LF5 Secondary: LF4, LF3	Up to 8.0 m	Axis, off-axis, or margin regions of slope channels under conditions of coarse-grained sediment bypass (Type 1 and Type 2 channel elements) and/or subsequent channel abandonment (Type 1 channel elements)	Type 1 and Type 2 channel elements	Overlies LFA1 in Type 1 channel elements; sometimes underlies all other lithofacies associations in Type 2 channel elements	Mutti and Normark (1987, 1991); Barton et al. (2010); Macauley and Hubbard (2013); Hubbard et al. (2014); Stevenson et al. (2015); Hubbard et al. (2020)
LFA5: Siltstone-dominated deposits (Fig. 5E)	Primary: LF6 Secondary: LF5, LF4	Up to 25.0 m	Overbank regions (e.g., levees, other non-channelized slope settings)	Overbank elements	Lateral and vertical transition to LFA3 and LFA4 with increased proximity to channel elements	Mutti and Normark (1987, 1991); Piper and Normark (2001); Di Celma et al. (2011); Kane and Hodgson (2011); Hansen et al. (2015, 2019)
LFA6: Disorganized and/or chaotically bedded deposits (Fig. 5F)	Primary: LF8 Secondary: LF7	Up to 15.0 m	Areas of submarine mass wasting	Mass-transport deposits	No systematic relationships observed	Hampton (1972); Middleton and Hampton (1973, 1976); Armitage et al. (2009); Auchter et al. (2016)

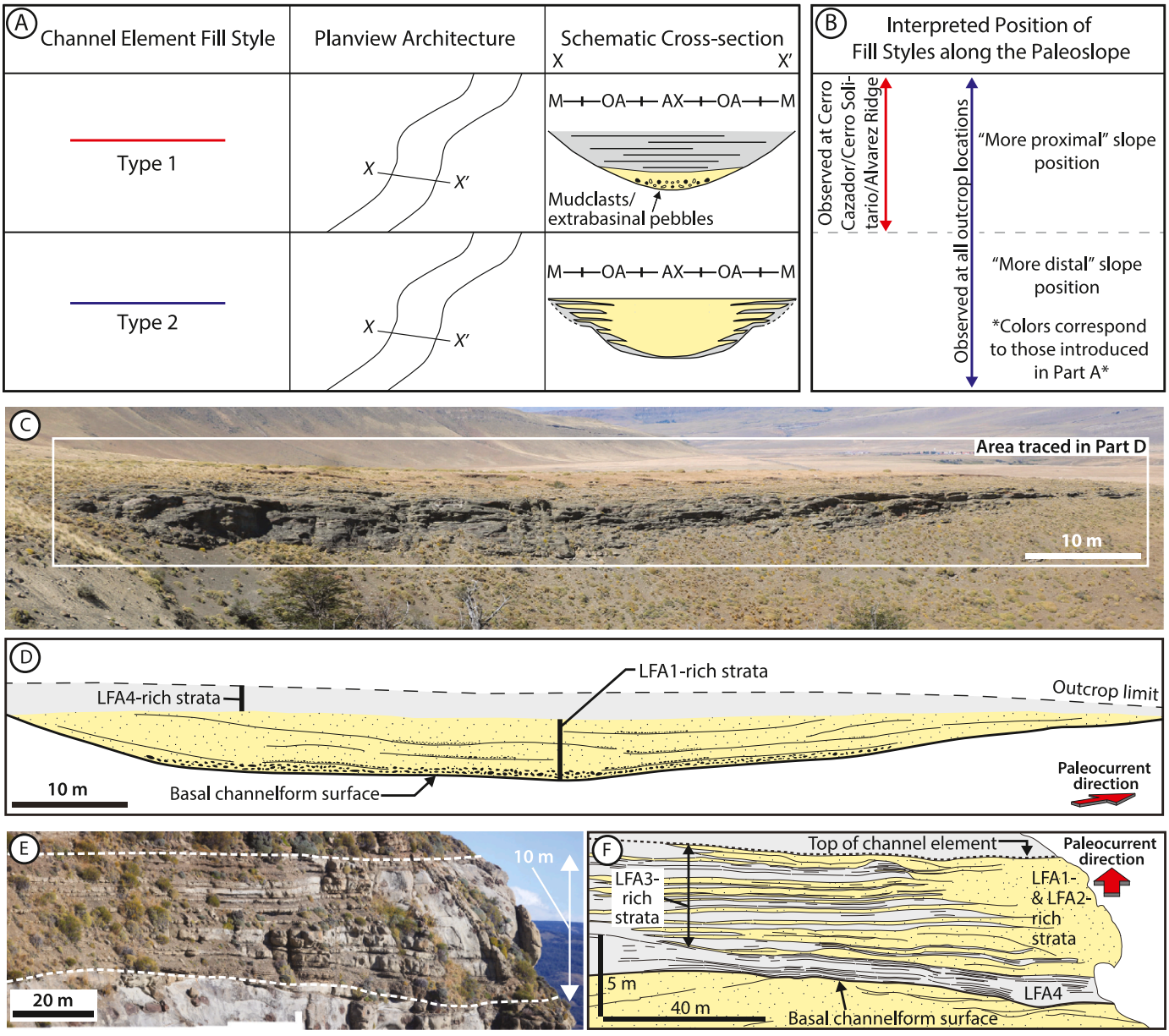

Fig. 6. (A) The spectrum of commonly documented channel element fill styles. In each schematic, sandstone is yellow and siltstone is gray. Each channel element is commonly 10–30 m thick and 150–400 m wide (channel elements shown in the diagram are 30 m thick and 400 m wide). The relative positions of the channel axis (AX), off-axis (OA), and margin (M) regions are indicated. Diagram modified from Pemberton et al. (2016). (B) Interpreted position of channel fill styles along the paleoslope. (C–F) Channel element architecture at various locations along the outcrop belt. In each trace diagram, sandstone-rich strata is yellow and siltstone-rich strata is gray. (C, D) Photograph and trace diagram of a Type 1 channel element exposed at Cerro Cazador. (E, F) Photograph and trace diagram of a Type 2 channel element at Laguna Figueroa. Modified from Macauley and Hubbard (2013).

2014). The occurrence of mass-transport deposits stratigraphically below packages of channel elements and overbank elements suggests that mass-wasting is linked to the formation of a conduit on the seafloor (cf. Deptuck et al., 2007; Bain and Hubbard, 2016; Ward et al., 2018; Cronin et al., 2022), and that the resulting seafloor topography affected subsequent sediment routing (Armitage et al., 2009; Kneller et al., 2016).

5.3. Complexes of fundamental elements

Analysis of the distribution of fundamental elements enabled identification of complexes (Fig. 8). Complexes were differentiated via documentation of abrupt shifts in element stacking deduced from a change in the nature of stacked lithofacies associations (e.g., shift from stacked channel axis deposits to out-of-channel deposits). Complexes discussed include: (1) channel complexes; and (2) mass-transport complexes. Due to vegetative cover along the outcrop belt, complexes of overbank elements could not be confidently delineated (Fig. 8).

5.3.1. Channel complexes

Description: Channel complexes are up to ~90 m thick and are up to ~1000 m wide in depositional cross-section where exposed (Fig. 8). Basal surfaces of channel complexes truncate underlying strata, and are often overlain by mass-transport deposits (Fig. 8). Above the mass-transport-deposit-dominated interval, channel complexes contain ≥2 Type 1 and/or Type 2 channel elements that stack in a consistent pattern. Stacking consistency is recognized via consideration of the trajectory and degree of lateral offset between successive channel

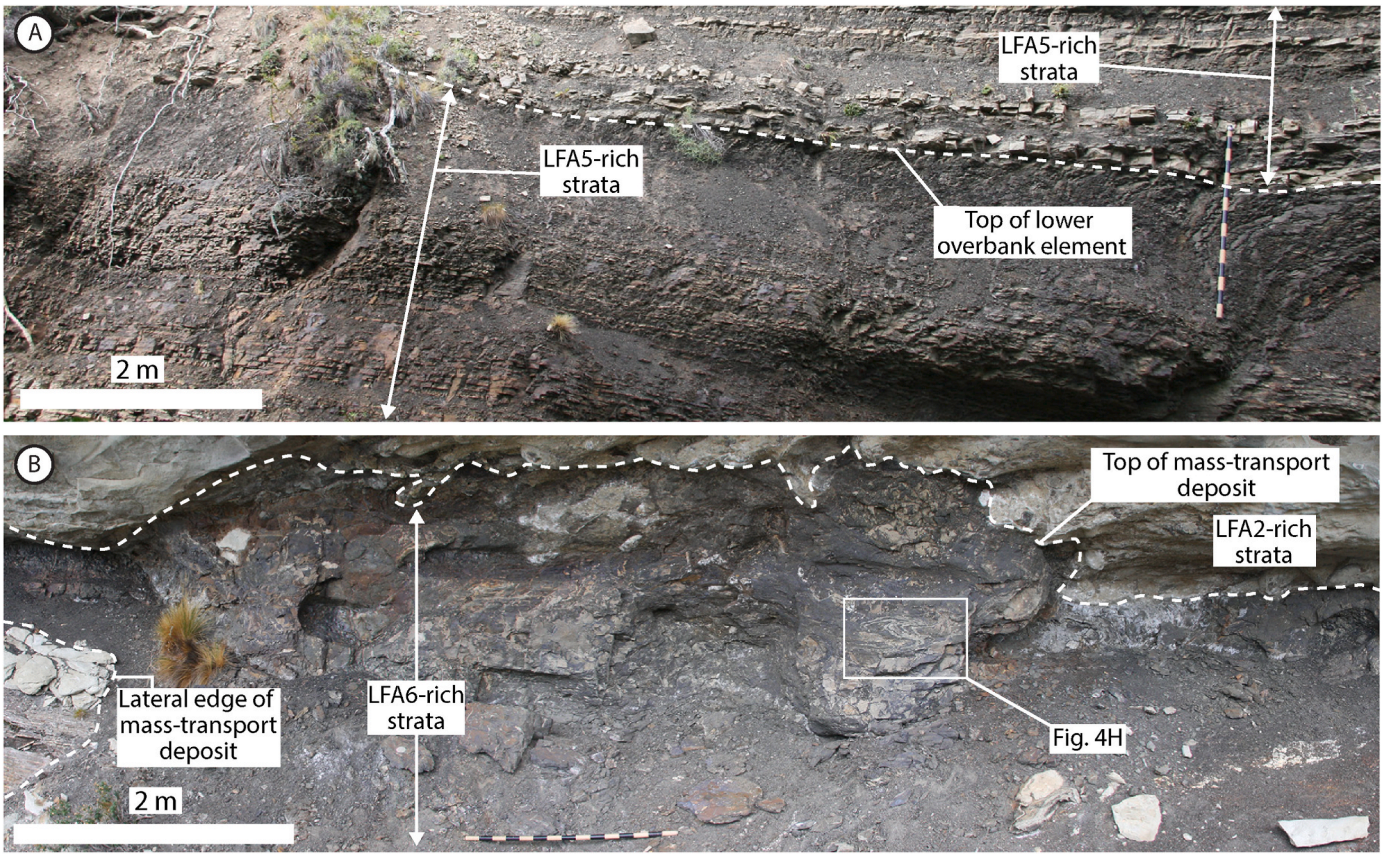

Fig. 7. Examples of architecture for overbank elements (A) and mass-transport deposits (B). Overbank elements in (A) contain LFA5-rich strata. The mass-transport deposit in (B) is characterized by chaotically bedded siltstone-rich deposits (i.e., LFA6-rich strata; Fig. 4H). Jacob's staff in (A) and (B) is 1.5 m long.

elements (Fig. 8). Stacking patterns vary considerably along the outcrop belt; in some cases, stacking is defined by high lateral offset between channel elements (i.e., early-stage channel complex, Fig. 8B), while in others, stacking is more laterally restricted (i.e., late-stage channel complex, Fig. 8B). Top surfaces of channel complexes are commonly flat (Fig. 8). Channel complexes are exposed at all outcrop locations.

Interpretation: Channel complexes record a phase of slope channel system evolution marked by consistent or systematic channel migration (McHargue et al., 2011). Channel complex thickness and width variations appear to correlate with changes in channel element stacking. Wider and thinner complexes (i.e., early-stage channel complex; Fig. 8B) are generally linked with marked lateral offset between successive channel elements, while narrower and thicker complexes (i.e., late-stage channel complex; Fig. 8B) are often linked with laterally restricted channel element stacking. Changes in channel element stacking patterns reflect variations in channel migration patterns, which are controlled by: (1) erosional confinement offered by the basal surface of the conduit (Cross et al., 2009; Jobe et al., 2011); and/or (2) constructional confinement from overbank units (e.g., Hübscher et al., 1997; Hodgson et al., 2011).

5.3.2. Mass-transport complexes

Description: Mass-transport complexes are present stratigraphically below thick intervals of stacked channel complexes (Fig. 8). Mass-transport complexes are at least 15 m thick and are 100s of m wide in depositional-strike cross-section where exposed (Fig. 8). Basal surfaces of mass-transport complexes can be highly irregular and exhibit marked truncation of underlying units (>10 m of erosional relief; Appendix B, Fig. B6). Mass-transport complexes are composed of ≥2 mass-transport deposits, where boundaries are often delineated by discontinuous sandstone units (Appendix B, Fig. B6). Mass-transport deposit stacking patterns in these complexes are highly irregular. The top surfaces of mass-transport complexes can display variable geometry, which is often controlled by truncation from overlying channel elements (Fig. 8). Though mass-transport complexes are present at all outcrop locations, the best exposed examples are seen at Alvarez Ridge and Laguna Figueroa (Fig. 8).

Interpretation: Mass-transport complexes record a phase of submarine mass-wasting (Frey-Martínez et al., 2006; Alves, 2015). The erosional nature of these complexes suggests that mass-wasting was related to creation of a channel-system-scale conduit through which turbidity currents were subsequently routed (Kneller et al., 2016; Cronin et al., 2022). It is plausible that the topography along the tops of these complexes provided the template for the evolution of stacking patterns observed in channel complexes (Peakall et al., 2000; Moscardelli et al., 2006).

5.4. Systems of complex-scale architectural elements

Analysis of the distribution of complexes enabled identification of three discrete channel systems (Channel Systems 0, 1, and 2), which are interpreted to contain genetically related complexes (Figs. 2, 8 and 9). Identification of channel systems informed construction of a stratigraphic framework (Fig. 9), and fostered systematic analysis of channel deposits along the outcrop belt (Figs. 10 and 11). This study is focused on Channel Systems 1 and 2 (Figs. 10 and 11). Detailed characterization of Channel System 0 was not undertaken due to limited outcrop exposure, locally (Fig. 9).

5.4.1. Channel systems

Description: Channel Systems 1 and 2 (Fig. 9) are up to ~150 m thick and ~2200 m wide; channel system dimensions are constrained by

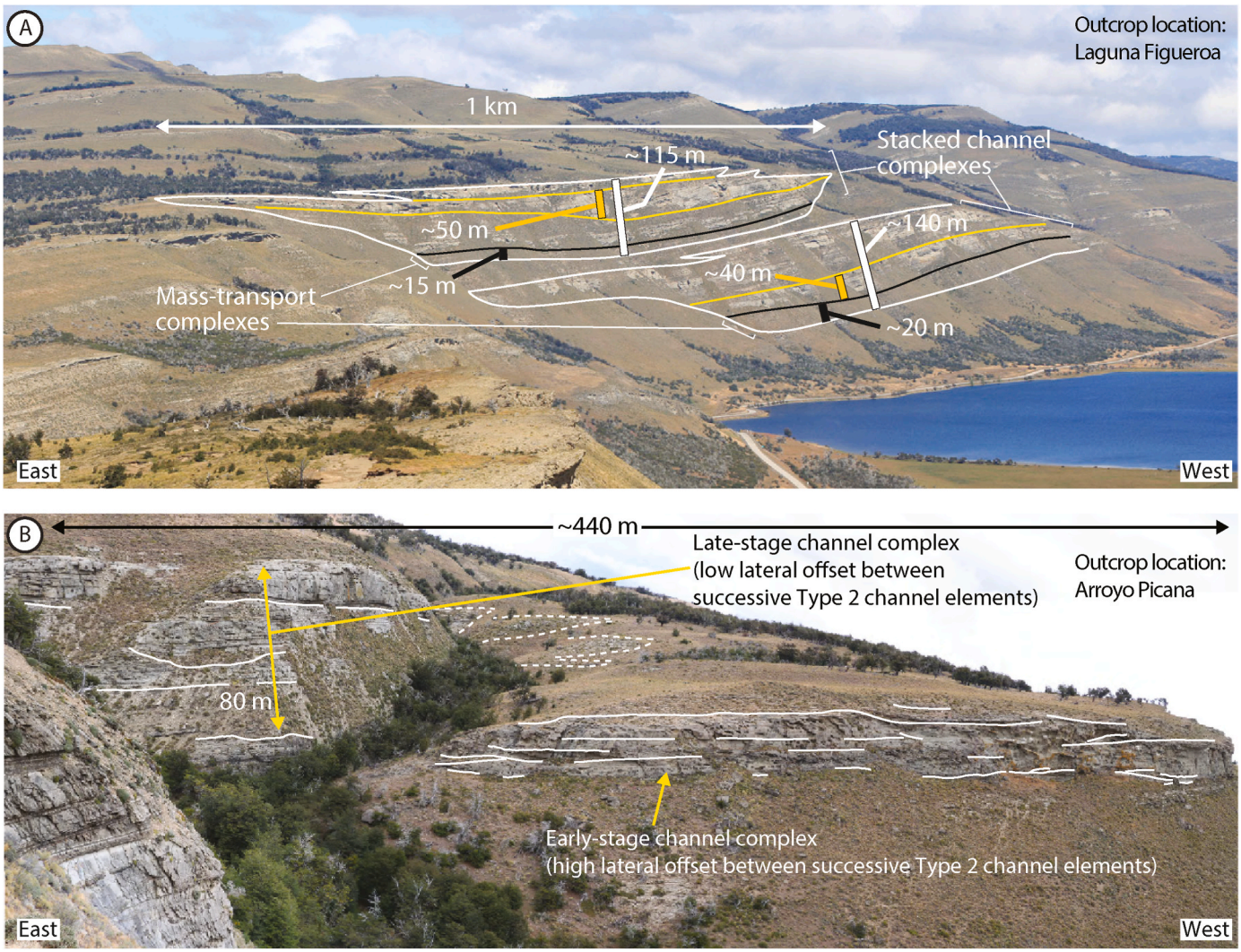

Fig. 8. (A) Outcrop examples of composite architectural elements. Paleocurrent direction is into the page. The boundaries of channel complexes and mass-transport complexes are indicated with orange and black lines respectively. Areas of channel systems that are dominated by channel complexes and mass transport complexes are indicated with white lines. Channel systems plausibly incorporate overbank elements that are adjacent to these areas (Fig. 2). Thicknesses for each of the aforementioned features are provided. (B) Channel element and channel complex stacking patterns within a channel system exposed at Arroyo Picana. Paleocurrent direction is into the page. A complex that is dominated by Type 2 channel elements that are significantly offset laterally is present towards the base of this channel system, while a complex that is dominated by laterally restricted Type 2 channel element stacking is present towards the top of this channel system.

direct outcrop observations (Fig. 9) and interpretive extrapolations (Figs. 10 and 11; Appendix A). Basal surfaces of these features are often highly irregular and erode deeply into underlying units (>10 m of relief). Channel systems often contain at least three distinct intervals of variable thickness, which include: (1) a mass-transport complex near the base (Fig. 8); (2) a channel complex defined by marked lateral offset between channel elements directly above the mass-transport complex (Fig. 8); and (3) one or more channel complexes defined by elevated aggradation and decreased lateral offset between channel elements towards the top (Fig. 8). Top surfaces of channel systems are often flat (Fig. 8).

Interpretation: Channel systems record the multi-phase history of a large submarine sediment-routing system, which includes: (1) the establishment of a channel-system-scale conduit via erosion and mass failure; (2) subsequent formation and filling of channels that are defined by high lateral mobility, and ultimately, high lateral offset between successive elements; and (3) later formation and filling of highly aggradational channels, recorded by lower lateral offset between successive elements. This evolutionary framework has been observed in many other ancient deep-water channel systems worldwide (e.g., Deptuck et al., 2003; Hodgson et al., 2011; Covault et al., 2016; Englert et al., 2020; Cronin et al., 2022). The general decrease in lateral offset between channel elements over the depositional history of the system has been attributed to: (1) an overall decrease in the size, caliber, and density of flows being routed to the system over time, which triggers a rise in equilibrium profile and promotes vertical aggradation of channel elements (McHargue et al., 2011; Jobe et al., 2015); and (2) growth of levees resulting from increased deposition of fine-grained detritus related to (1), which progressively increases accommodation in portions of the conduit, promoting subsequent channel development (Hodgson et al., 2011).

6. Downslope changes in slope channel fill and stacking patterns

Establishment of the stratigraphic framework combined with context afforded by larger-scale clinoform mapping (Hubbard et al., 2010; Bauer et al., 2020) enabled characterization of downslope trends in channel fill and stacking patterns for channel elements, channel complexes, and channel systems (Fig. 10). Characterization of downslope changes in

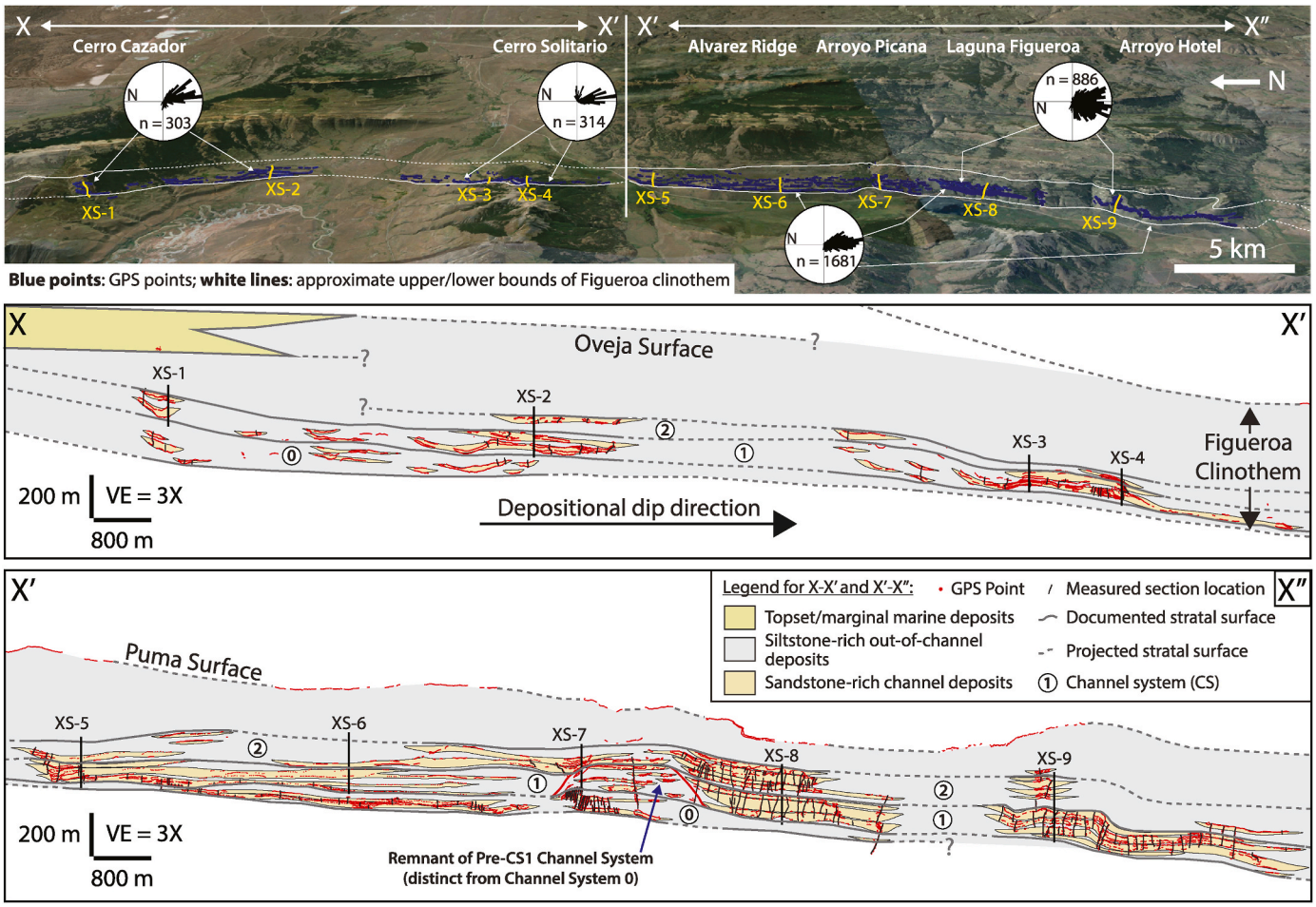

Fig. 9. Overview of stratigraphic architecture associated with slope channel systems preserved in the Figueroa clinothem. The top image shows the geographic extent of outcropping features associated with the Figueroa clinothem (image data: Google, CNES, Astrium, DigitalGlobe, Landsat, Copernicus, 2016; center of image coordinates: 51°17′46.44″S, 72°22′42.65″W). Paleocurrent data is derived from Daniels et al. (2018) and references therein. Depositional-dip-oriented cross-sections of the clinothem are shown in X-X′ and X′-X′′. Stratigraphic correlations enable identification of three distinct channel systems that crop out along the length of the transect. The apparently discontinuous nature of some of the sandstone bodies is due to the sinuous nature of the formation of slope channels. Some point sets and geobodies appear deformed on the correlation panel; this is a result of localized structural deformation along the outcrop belt that was not removed during point projection. Lines denoted by "XS" refer to locations where depositional-strike-oriented cross-sections were constructed to evaluate along-dip changes in channel fill stacking patterns (see Figs. 10 and 11).

channel fill and stacking patterns involved comparison of net-to-gross values from outcrop and subsurface data sets to investigate sandstone proportion trends across a wide array of systems.

6.1. Channel elements

6.1.1. Results

Changes in the prevalence of Type 1 and Type 2 channel elements are observed down-paleoslope within each studied channel system (Fig. 10). In updip regions (e.g., XS-1, XS-2; Fig. 10), Type 1 and Type 2 channel elements are observed; Type 1 channel elements account for nearly half of the observed elements in some locations (i.e., XS-2). In downdip regions (e.g., XS-7 to XS-9; Fig. 10), only Type 2 channel elements are present. Due to the elongated nature of the outcrop and common depositional-dip- or oblique-dip-oriented exposures, systematic down-slope changes in channel element width are difficult to constrain.

Channel element net-to-gross values from stratigraphic sections range from 15% to 100% (Appendix A); however, most values exceed 40% (Fig. 12A). The mean and median channel element net-to-gross values in Channel System 1 increase downdip; mean values increase from ~67% at Cerro Cazador to ~86% at Arroyo Hotel, while median values increase from ~80% to ~90% at those localities (Fig. 12A). These trends are accompanied by an overall narrowing of the interquartile (25th-75th percentile) range and full range of values in the data set downdip, which is dominated by higher net-to-gross values (>80%) towards Arroyo Hotel (Fig. 12A). Channel element net-to-gross trends for Channel System 2 elements are similar to those from Channel System 1. For Channel System 2, mean values increase from ~67% at Cerro Cazador to ~88% at Arroyo Hotel, while median values increase from ~65% to ~97% at those localities (Fig. 12A).

Channel element net-to-gross data from outcrop were considered alongside data from the Pliocene Giza North channel system offshore of Egypt (Morris et al., 2014, Fig. 12A). Net-to-gross values that were computed using our calculation methods spanned 36–90% for Giza North channel elements (Fig. 12A).

6.1.2. Interpretations

The presence of Type 1 channel elements in the updip zones of Tres Pasos Formation channel systems reflects a higher degree of coarse-grained sediment bypass in those areas (Mutti and Normark, 1987), while the prevalence of Type 2 channel elements downdip suggests increased in-channel deposition of coarse-grained sediment down-paleoslope (Figs. 9 and 10). These interpretations are supported by net-to-gross values, which suggest an increase in intra-element

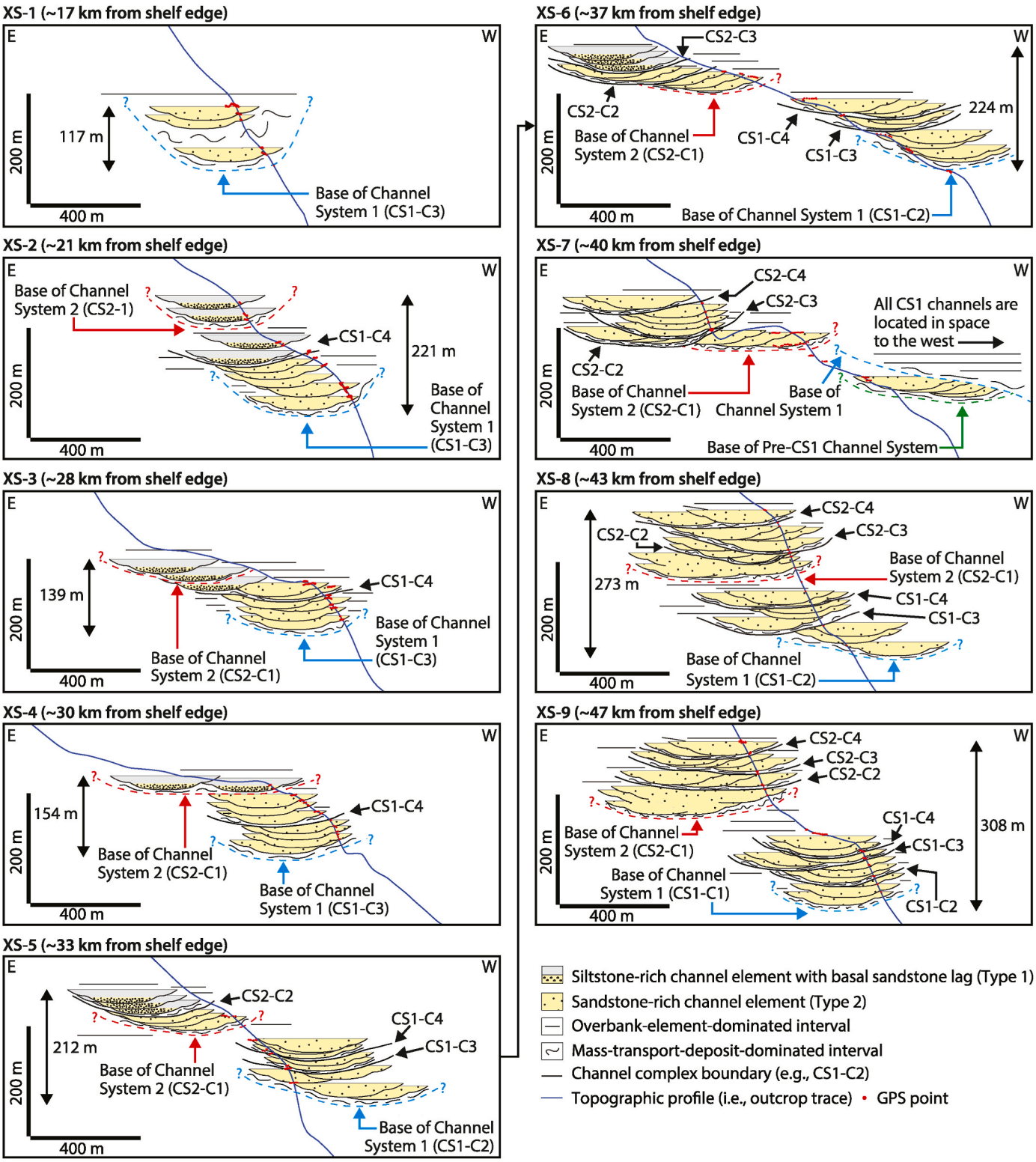

Fig. 10. Depositional-strike-oriented cross-sections that show channel element stacking patterns in the context of interpreted composite channelform bodies (i.e., channel complexes, channel systems). Siltstone-rich channel elements (i.e., Type 1) are not documented in cross-sections located south of XS-6; this suggests that coarse-grained sediment bypass was an important process in the paleoslope regions located north of XS-7. In these diagrams, individual channel fills are 25 m thick and 400 m wide; these dimensions are based on the average of the maximum channel element thicknesses documented at the various outcrop locations, as well as estimates for the widths of Tres Pasos Formation slope channels reported by previous workers (i.e., Hubbard et al., 2014). Dashed lines present near the bottom of each channel system in each stacking pattern diagram represent the base of an interval of mass-transport deposits. The lowest point along each of these lines (indicated with a red or blue arrow) is interpreted to closely coincide with the position of the master bounding surface associated with a given channel system. Fine-scale architecture associated with Type 1 and Type 2 channel elements is not shown in these diagrams. Distances from the shelf edge were inferred using the position of each cross-section in relation to the position of the Figueroa clinoform shelf edge featured on the regional stratigraphic cross-section shown by Daniels et al. (2018). CS—channel system; C—channel complex.

sandstone content downdip in both systems (Fig. 12A). Enhanced deposition of coarse-grained detritus in downdip areas has been reported in other deep-water slope systems globally (e.g., Saller et al., 2004; Houseknecht et al., 2009; Covault et al., 2012). Though various flow properties, such as flow size, caliber, and density, affect the degree of bypass along slopes (Mutti, 1992; Heijnen et al., 2022), it is plausible that the prevalence of Type 2 channel elements downdip is mainly linked to a decrease in average slope gradient downdip, promoting deposition of coarse-grained detritus as individual flows waned (Fig. 1; Stevenson et al., 2015).

6.2. Channel complexes

6.2.1. Results

Channel complexes exhibit changes in fill and stacking patterns along the paleoslope (Fig. 10). In updip regions (XS-1; Fig. 10), the sole channel complex documented (CS1–C3) contains three Type 2 channel elements that are present amongst a thick interval of mass-transport deposits (Fig. 10). Down-paleoslope, the number of documented channel complexes within each channel system increases (e.g., XS-5 to XS-9; Fig. 10); channel complexes in these regions are often defined by thick intervals of amalgamated Type 2 channel elements. Channel element stacking within complexes is defined by high lateral offset in some locations (e.g., CS1–C2; XS-8; Fig. 10), and low lateral offset in others (e.g., CS1–C4; XS-9; Fig. 10).

Analysis of down-paleoslope trends in net-to-gross was performed for complexes in Channel System 1, leveraging near-complete exposures along the outcrop belt (Figs. 9 and 12B). Channel complex net-to-gross values in the updip areas of Channel System 1 generally range from ~37% to 67% (Cerro Cazador and Cerro Solitario; Fig. 12B). Net-to-gross values in downdip regions are higher, spanning ~60–97%. Most values from Channel System 1 are within the range of complex net-to-gross values from Channel System 2, which span ~45–98% (Fig. 12B).

Net-to-gross data from outcropping channel complexes were compared with data from channel complexes in the subsurface offshore of Angola (Porter et al., 2006), Brazil (Fowler and Novakovic, 2018), Tanzania (Sansom, 2018), and Egypt (Cross et al., 2009; Morris et al., 2014). Net-to-gross values from subsurface channel complexes that were computed using our calculation methods are highly variable, spanning 26–100% (Fig. 12B).

6.2.2. Interpretations

Fill and stacking pattern variations within channel complexes along the paleoslope are attributable to autogenic processes (Sylvester et al.,

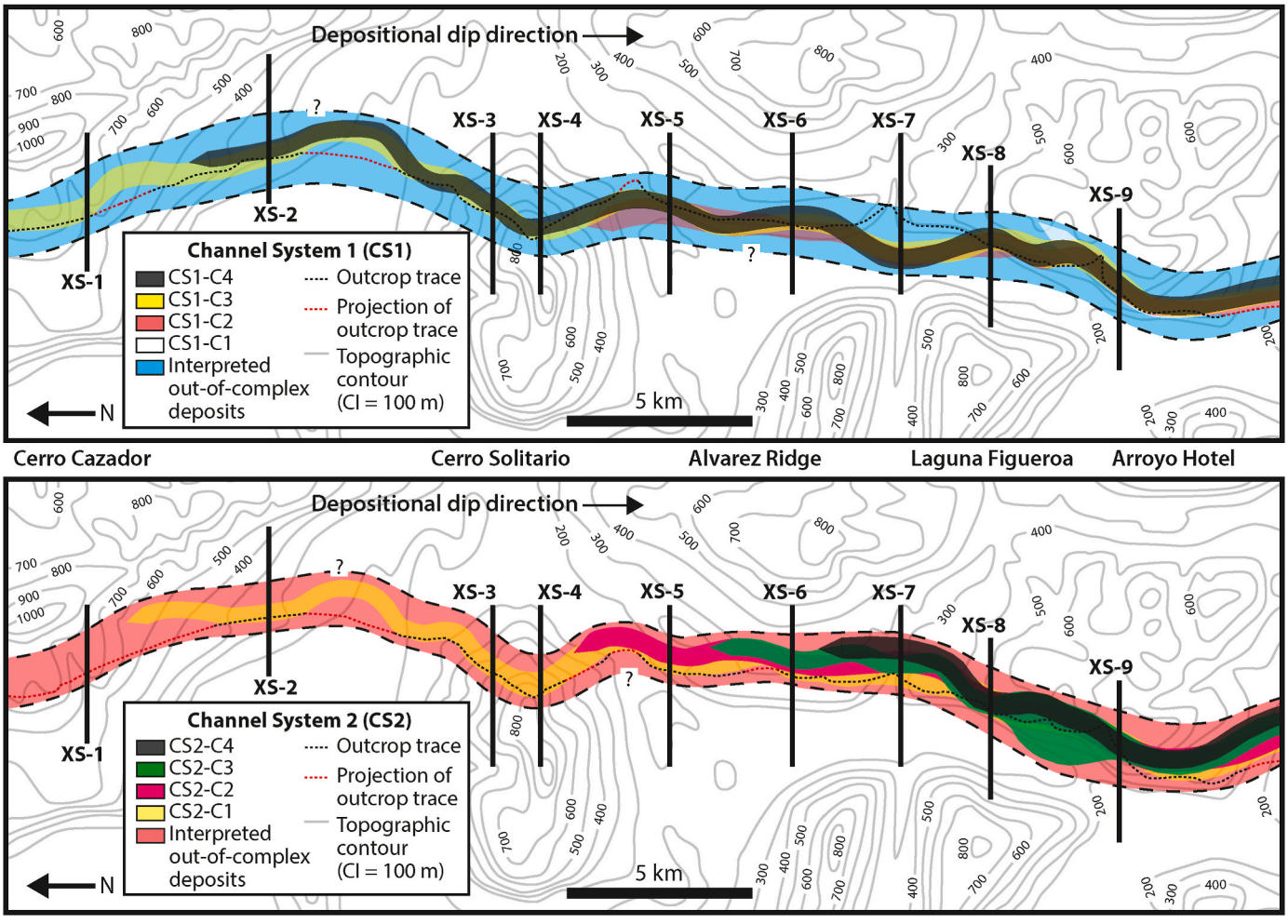

Fig. 11. Along-slope planform correlation of Channel Systems 1 and 2. In each diagram, channel complex widths are considered minimum widths, and are constrained by observations and interpretations associated with channel element stacking patterns that are shown in depositional-strike-oriented cross-sections (e.g., XS-1) in Fig. 10. Channel complexes taper where it is not possible to map sandstone-rich intervals within them any farther (e.g., upslope regions). Channel system boundaries (thick black dashed lines) are largely based on interpretive extrapolations from available outcrop exposure; however, at outcrop locations where a given channel system contained more than one channel complex, channel system width was estimated using the thickness of the system as a guide (see Fig. 3 for an overview of the methodology associated with this approach). Topographic contours were extracted from a differential-GPS-based digital elevation model generated using Petrel software (Schlumberger, 2014). CS—channel system; C—channel complex.

2012), driven by factors such as sinuosity development amongst successive channels. However, other factors such as mass-wasting, as well as enhanced coarse-grained sediment bypass in updip regions of the system and increased coarse-grained sediment deposition in downdip regions of the system, can also play a role (Saller and Dharmasamadhi, 2012). As with channel elements, these changes are likely linked to an overall decrease in average slope gradient downdip. Channel element stacking pattern variability is controlled by: (1) confinement offered by the surface that defines the boundaries of the conduit on the seafloor; (2) relief from adjacent overbank units; and (3) mass-wasting within the conduit, which can impact the lateral and vertical offset between successive elements (Fig. 10; Janocko et al., 2013; Bain and Hubbard, 2016). Net-to-gross values at this scale are tied to: (1) channel element net-to-gross, which is linked to the degree of coarse-grained sediment bypass occurring at a given along-slope position, and (2) channel element stacking patterns, as net-to-gross values from channel complex intervals that incorporate thick packages of siltstone-rich out-of-channel deposits will be lower than for intervals that are mainly composed of sandstone-rich channel elements (Fig. 10).

6.3. Channel systems

6.3.1. Results

Sandstone-rich intervals in the studied Tres Pasos Formation channel systems generally become thicker and more amalgamated downpaleoslope (i.e., XS-8, XS-9; Fig. 10); however, changes in the thickness and the degree of amalgamation of sandstone-rich intervals can be quite irregular between adjacent outcrop locations (i.e., CS1 from XS-2 to XS-4; Fig. 10). Channel complex stacking patterns within channel systems are highly variable, owing to channel element stacking pattern changes along the paleoslope (Figs. 10 and 11). Net-to-gross values reveal marked along-strike variability in sandstone proportion at all paleoslope positions (Fig. 13). Maximum net-to-gross values for Channel Systems 1 and 2 vary markedly along the paleoslope (range of maximum

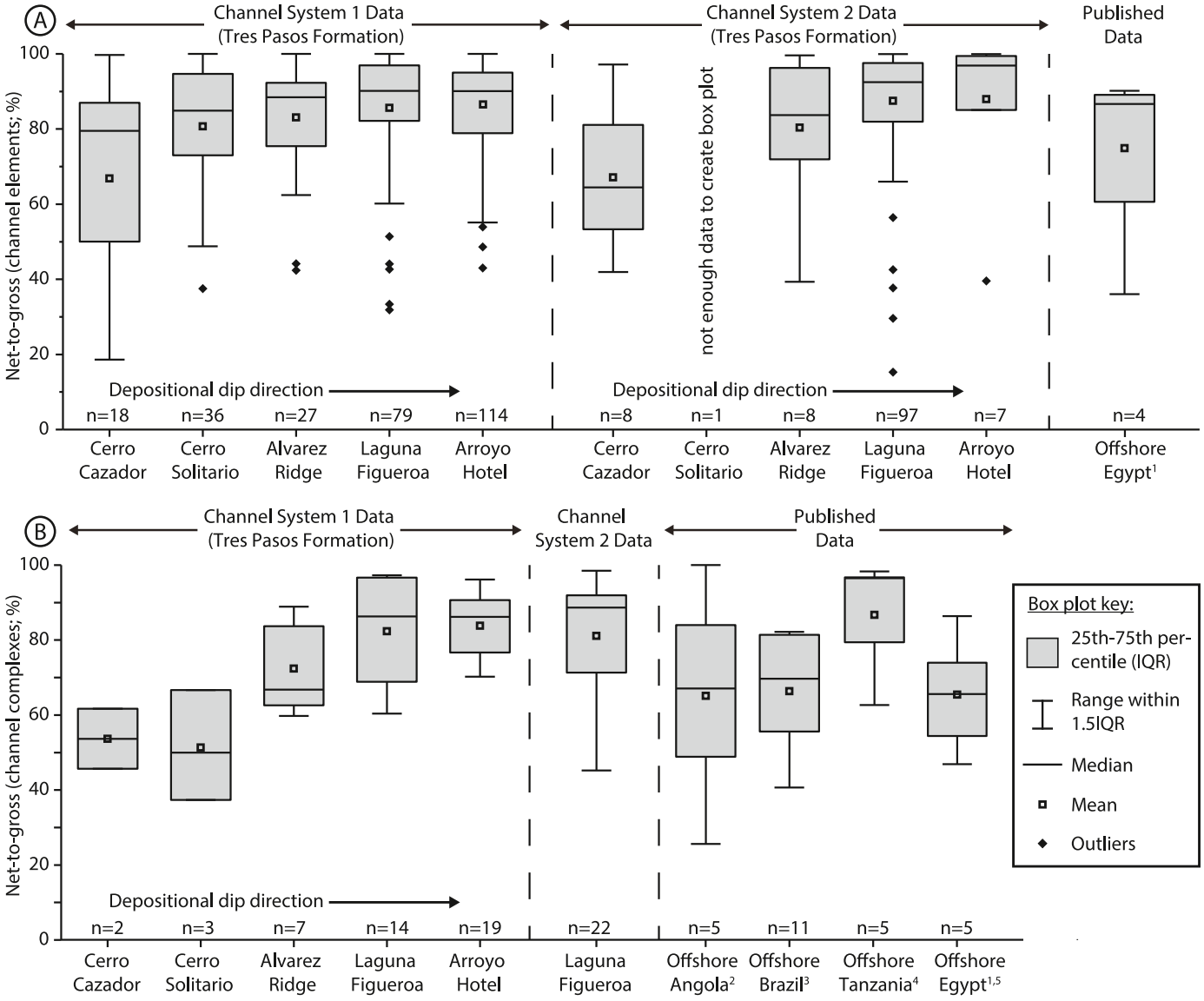

Fig. 12. Box plots that illustrate the range of net-to-gross values for channel elements (A) and channel complexes (B) in Channel System 1 and Channel System 2 of the Tres Pasos Formation, as well as for subsurface data sets (see Appendix A for all raw data). For data from the Tres Pasos Formation, each label on the x-axis of each plot corresponds to an outcrop location shown in Fig. 1. Data sources associated with published data sets are as follows: (1) Morris et al. (2014); (2) Porter et al. (2006); (3) Fowler and Novakovic (2018); (4) Sansom (2018); and (5) Cross et al. (2009). Net-to-gross values from subsurface data sets utilize interpretations presented in each study (see Appendix A), which are based on core descriptions (data sources 1, 2, 4, 5) as well as petrophysical logs (data sources 1, 2, 3, 4, 5). n—number of channel element/complex intervals used in box plots; IQR—interquartile range.

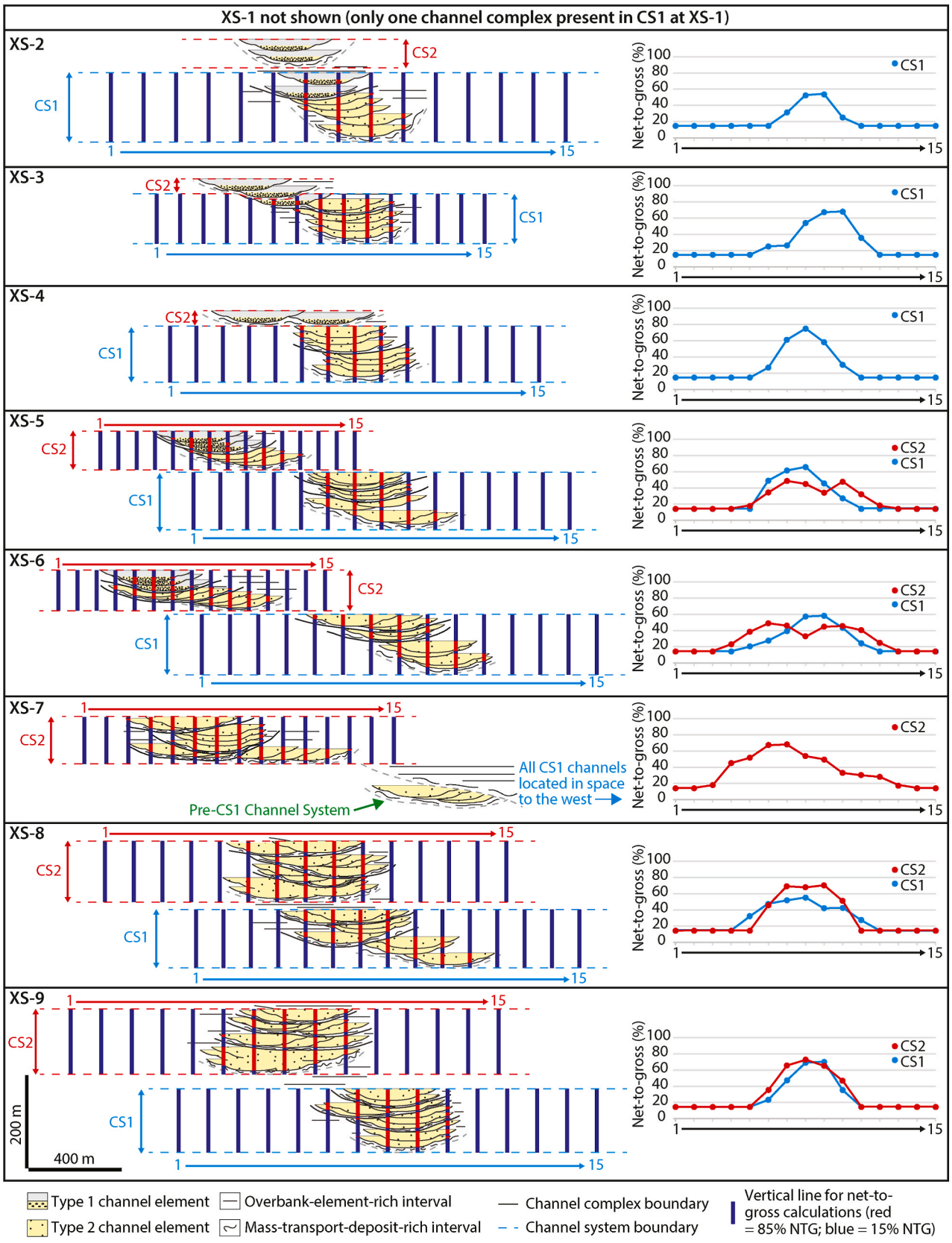

Fig. 13. Net-to-gross (NTG) results for channel systems associated with stacking pattern diagrams from the Figueroa clinothem. For Type 1 channel elements, sandstone-rich areas were assigned an 85% net-to-gross ratio, and siltstone-rich areas were assigned a 15% net-to-gross ratio (see text for further explanation). For Type 2 channel elements, all areas were assigned a 85% net-to-gross ratio. Net-to-gross calculations were not performed for channel systems in cases where only one channel complex was present at a given cross-section location. Numbers above each vertical line in each channel system refer to along-depositional-strike positions featured in Fig. 15A and 15B.

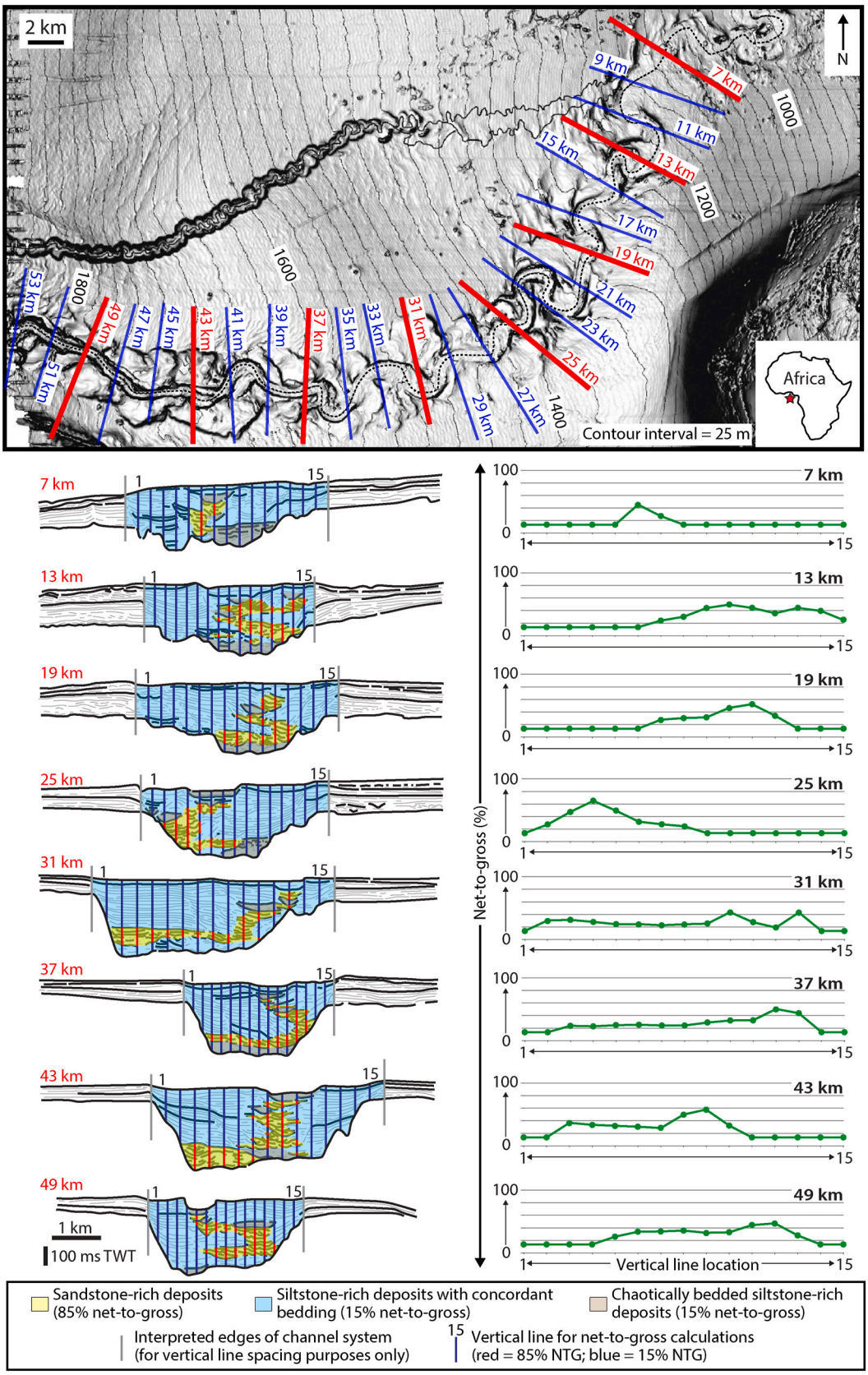

Fig. 14. Channel element stacking patterns and net-to-gross data associated with the Benin-major channel system, offshore Nigeria. Red lines in the upper image show the locations of depositional-strike-oriented cross-sections shown in the lower part of the figure; blue lines show the locations of additional cross-sections analyzed in this study, which are featured in Appendix C. In each cross-section, high-amplitude reflections are indicated with thick black lines, while low-amplitude reflections are indicated with thinner gray lines. Modified from Deptuck et al. (2007).

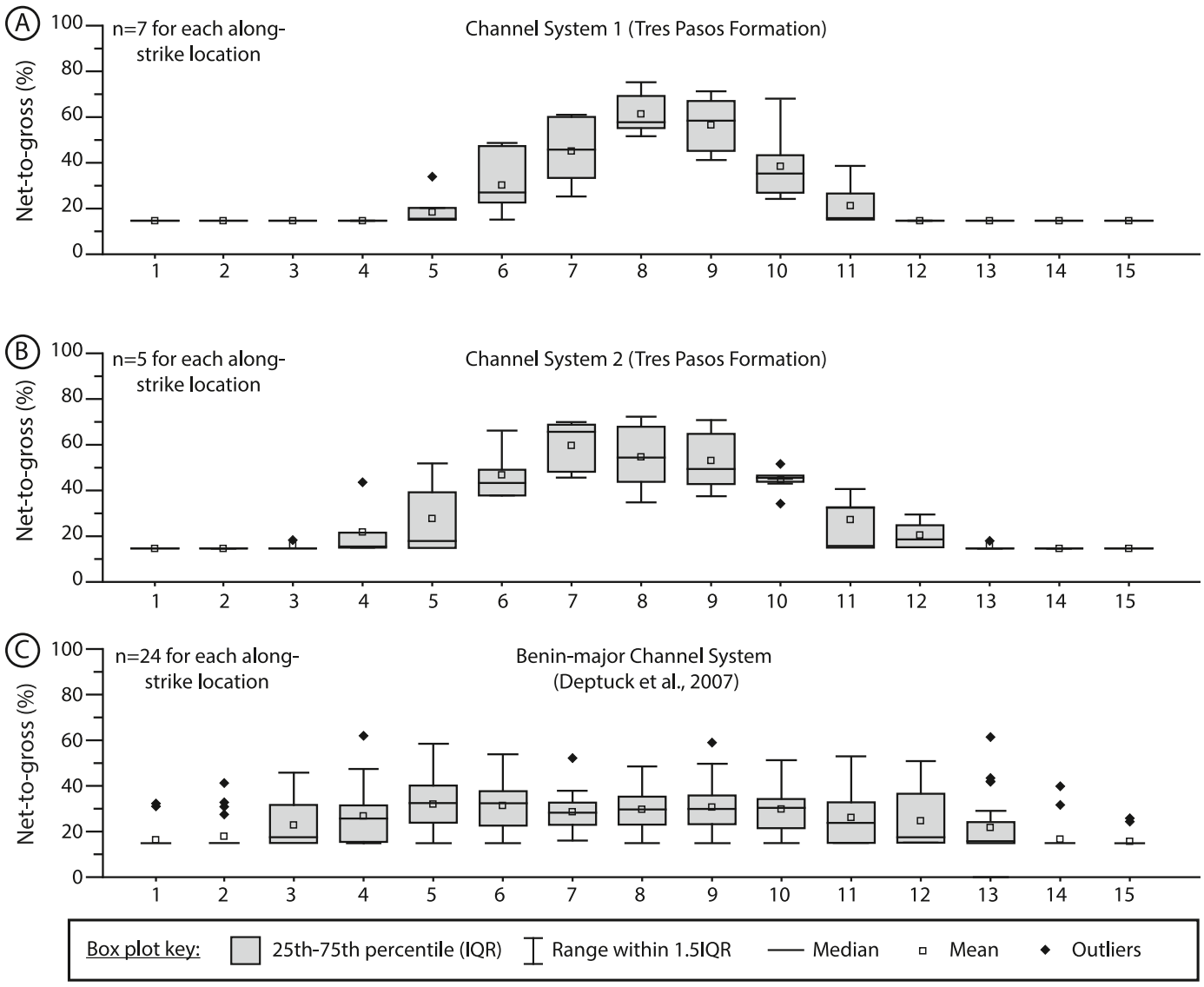

Fig. 15. Summary of channel system net-to-gross values from outcrop and subsurface data sets. (A, B) Compilation of channel system net-to-gross values from the Tres Pasos Formation (see Appendix A for raw data). Numbers on the x-axis correspond to vertical line locations in Fig. 13. Box plots were created via combining all data points associated with a given along-strike location (i.e., vertical line location 1) from all cross-sections (Fig. 13). (C) Compilation of the range of net-to-gross values from each cross-section from the Benin-major channel system (see Appendix A for raw data). Numbers on the x-axis refer to vertical line locations in each cross-section from Fig. 14 and Appendix C. Box plots were created via combining all data points associated with a given along-strike location (i.e., vertical line location 1) from all cross-sections (Appendix C). n—number of data points used to construct box plots; IQR—interquartile range.

values at each cross-section location for both systems: 48–75%; Appendix A); notably, the highest values are associated with intervals of vertically stacked sandstone-rich channel elements. However, since these intervals can be found in both updip and downdip locations (e.g., CS1 at XS-3; Fig. 13), a systematic relationship between channel system net-to-gross and paleoslope position is not evident.

Along-strike variability in net-to-gross values for the Benin-major channel system is notable at each cross-section location (Fig. 14). Maximum net-to-gross estimates for the Benin-major system are highly variable down-paleoslope (range of maximum values at each cross-section location: 38–62%; Fig. 14; Appendix C), and systematic relationships between net-to-gross values and paleoslope position are not apparent.

6.3.2. *Interpretations*

Sandstone proportion trends at this scale are related to: (1) the degree of coarse-grained sediment bypass occurring at a given point on the slope; and (2) architectural element stacking patterns, which control the along-strike variability at each cross-section location (Fig. 14). The lower range of net-to-gross values for channel systems as compared to the range of values for channel elements and channel complexes (Figs. 15 and 16) is tied to the larger amount of siltstone-rich overbank units incorporated into channel systems (Fig. 2). Though Tres Pasos Formation observations suggest that channel systems may be characterized by an increased proportion of sandstone-rich channel elements downdip, observations from the Benin-major system imply that these trends may not always be systematic in other cases (Appendix C). The removal of coarse-grained units along certain regions of the slope via mass-wasting, or more substantial variations in element stacking patterns, may confound identification of linkages between sandstone proportion and slope position at this scale.

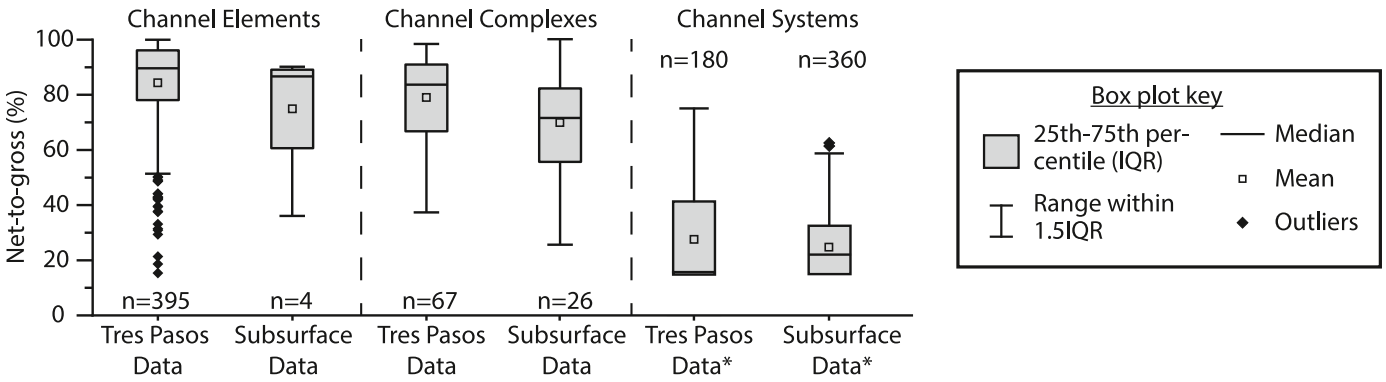

Fig. 16. Comparison of the net-to-gross ranges for channel elements, channel complexes, and channel systems for outcrop and subsurface data sets featured in this study. Sources of subsurface data include Porter et al. (2006), Deptuck et al. (2007), Cross et al. (2009), Morris et al. (2014), Fowler and Novakovic (2018), and Sansom (2018). Asterisks are used to denote data distributions that were not directly obtained from measured section, core, or wireline log data (see text for explanation). n—number of data points used to construct box plots; IQR—interquartile range.

7. Discussion

7.1. Controls on the downslope distribution of coarse-grained sediment

The downslope distribution of coarse-grained sediment within channel elements is tied to the sedimentary processes involved in the sculpting and filling of slope channels (Mutti and Normark, 1987). A higher degree of coarse-grained sediment bypass within channels in the updip areas (XS-1, XS-2; Figs. 9 and 10) of the Tres Pasos Formation channel system resulted in the development of siltstone-rich channel elements with thin intervals of coarse-grained material in those regions (i.e., Type 1 channel elements at XS-2; Fig. 10). Increased in-channel deposition of coarse-grained sediment is recorded in downdip areas by the prevalence of sandstone-rich (i.e., Type 2) channel elements in those regions (Fig. 10). It has been shown that the propensity for coarse-grained sediment bypass or deposition within slope channels is mainly controlled by the properties of turbidity currents (i.e., sediment concentration, grain size) routing sediment through the system, as well as slope gradient (e.g., Stevenson et al., 2015; Crisóstomo-Figueroa et al., 2021; Heijnen et al., 2022; Pope et al., 2022). Though the results of this study suggest that the documented changes in channel element fill are likely associated with an overall decrease in slope gradient downdip (Fig. 1), it is plausible that changes to flow properties may have also contributed to the lithologic variations observed (cf. McHargue et al., 2011).

The downslope distribution of coarse-grained sediment within channel complexes and channel systems is linked to the propensity for development of thick successions of sandstone-rich channel elements along-depositional-dip (Fig. 10), as well as channel element stacking patterns. While analysis of the average slope gradient of a system may inform crude prediction of downslope sandstone proportion trends at these scales, the results of this study suggest that thorough consideration of the topographic profile of a slope is required to more accurately predict downslope sandstone proportion trends and channel element stacking patterns for composite channelform bodies (Covault et al., 2012). As an example, slopes with smooth topographic profiles (e.g., prograding slopes in largely tectonically quiescent settings; Greenlee et al., 1992; Houseknecht et al., 2009) may promote a systematic shift from siltstone-rich channel complexes and systems in updip regions to sandstone-rich complexes and systems in downdip regions as the slope gradient predictably decreases. In this scenario, channel element stacking patterns may become less laterally restricted downdip as erosional confinement present in updip regions is lost (e.g., Saller and Dharmasamadhi, 2012); however, stacking patterns in downdip regions may also be governed by the degree of constructional confinement associated with overbank units, as well as the autogenic migration history of the channels (Labourdette and Bez, 2010; Hodgson et al., 2011). In contrast, slopes with highly irregular topographic profiles (e.g., slopes in tectonically active settings; Heiniö and Davies, 2007; Kendell, 2012) may exhibit marked changes in slope gradient over tens of kilometers (Beaubouef and Friedmann, 2000; Gee and Gawthorpe, 2006). Variable slope gradients promote irregular stacking pattern variations and sandstone richness trends, as numerous intraslope regions may be dominated by erosion and coarse-grained sediment bypass (e.g., high gradient slopes at the heads of slope minibasins; Beaubouef and Friedmann, 2000), while others may be dominated by coarse-grained sediment deposition (i.e., low gradient regions within slope minibasins; Beaubouef and Friedmann, 2000). These considerations emphasize the value of documenting the geologic history of deep-water slope systems when evaluating sandstone content and stacking patterns, as many geologic processes, including autogenic (e.g., shelf edge delta lobe avulsion; autogenic slope oversteepening and mass-failure) and allogenic mechanisms (e.g., tectonism), can affect the profile of any deep-water slope (Romans and Graham, 2013).

All of the aforementioned controls on the distribution of coarse-grained sediment along deep-water slopes are expected to apply to slopes that develop in a variety of tectonic settings. As a result, it is plausible that if two deep-water slopes in different tectonic settings possessed analogous characteristics (e.g., relief, gradient, topographic profile, run-out length), and the turbidity currents that were routed through those systems were similar, downslope changes in sandstone proportion in both systems may follow similar trends. Because the foredeep of the Magallanes-Austral Basin developed atop attenuated lithosphere (Fosdick et al., 2014), deep-water slopes of the Figueroa clinothem have characteristics that resemble deep-water slopes on passive continental margins (e.g., the Nigeria X slope system; Covault et al., 2012). In particular, the basin was >1 km deep, yielding long run-out channels that developed channelized stratigraphy shown to be analogous in scale and character to ancient deep-water channel systems on continental margins globally (e.g., Macauley and Hubbard, 2013; Reimchen et al., 2016; Meirovitz et al., 2020). As a result, sandstone proportion trends for slope channel systems of the Figueroa clinothem could aid with prediction of sandstone proportion trends for other systems with similar morphometric characteristics worldwide.

7.2. Application of computed net-to-gross values to reservoir prediction

7.2.1. Relationships between net-to-gross values and reservoir connectivity

For all net-to-gross calculations reported in this study, net thickness values were calculated using the total thickness of all coarse-grained units (e.g., sandstone) documented within a stratigraphic interval. This approach has been employed in many studies that aim to use net-to-gross values as a way to predict reservoir connectivity and performance, as high-quality natural resource reservoirs frequently consist of thick

and continuous sandstone-rich units in many areas worldwide (e.g., Samuel et al., 2003; Dailly et al., 2012; Mayall and Kneller, 2021). While linking high net sandstone thicknesses to highly prospective reservoirs has proven to be a successful exploration strategy in many instances (e.g., Sullivan et al., 2000; Mayall et al., 2006; Cronin et al., 2022), there are many other factors that can affect the ability of a sandstone-rich unit to act as a high-quality reservoir. As an example, Bell et al. (2018) showed that porosity and permeability within discrete sandstone-rich units in deep-water slope channel fills is primarily tied to: (1) the grain size distribution in each sandstone-rich unit; and (2) the proportion of detrital clay-sized material within the matrix of each unit. In cases where sandstone-rich units were dominantly coarse-grained and contained little detrital matrix material, porosity and permeability were found to be higher overall (Bell et al., 2018). However, even in situations where favourable porosity and permeability conditions exist in sandstone-rich units, other lithologic accessories (e.g., mudstone intraclasts) may be present and act as baffles or even barriers to flow (Mayall and Kneller, 2021). In many cases, such grain-scale textural aspects are not systematically characterized and a net-to-gross calculation emphasizes the presence and abundance of sandstone or sandstone-rich deposits (e.g., the calculation approach used in this study). As a result, establishing a direct link between high net-to-gross values and strong reservoir performance may prove challenging in some instances.

Architectural variations between discrete sandstone-rich units will also impact connectivity (Alpak et al., 2013; Jackson et al., 2019). As a demonstration of this point, consider an interval of stacked non-amalgamated sandstone-rich deposits from the Tres Pasos Formation. Though this interval may yield a high net-to-gross value, individual sandstone beds will be separated by thin siltstone-rich beds (Fig. 6). These intervals do not markedly impact net-to-gross values and are sub-seismic in scale, and therefore can be overlooked in subsurface studies with limited well control (Barton et al., 2010).

7.2.2. Relationships between net-to-gross values and slope channel hierarchy

Net-to-gross values reveal that measures of sandstone proportion are tied to hierarchical order, as channel elements and channel complexes tend to yield higher net-to-gross values than channel-system-scale bodies (Fig. 16). This is due to the increased proportion of siltstone-rich out-of-channel deposits that are included in net-to-gross calculations at larger scales (Fig. 2). Given this relationship, it is plausible that the featured compilation of net-to-gross values (Fig. 16; Appendix A) could inform forecasting of sandstone proportion trends at various scales in other analogous slope channel system reservoirs. This application may be especially valuable for systems that lack abundant data, and may be used to help estimate initial reservoir volumes.

The hierarchical framework used in this study to distinguish individual channel elements and composite channelform bodies (i.e., channel complexes and channel systems) is broadly comparable to the hierarchical schemes proposed by Pickering et al. (1995), Beaubouef et al. (1999), Sprague et al. (2002, 2005), Di Celma et al. (2011), McHargue et al. (2011), and Pickering and Cantalejo (2015). This framework was employed because it has been used by previous workers to characterize deep-water slope channel fills in other parts of the Tres Pasos Formation (e.g., Macauley and Hubbard, 2013; Hubbard et al., 2014). While many other published deep-water slope channel hierarchical frameworks identify similar orders of slope channel fill architecture (e.g., individual channel fills and composite channelform bodies), there can be considerable variation in: (1) the width and thickness of architectural elements linked to each order; and (2) the facies and stratigraphic architecture thought to be characteristic of each order (see Cullis et al., 2018 for a comprehensive review of hierarchical frameworks). Given this variability, we acknowledge that the net-to-gross values reported here may only be immediately applicable to other systems that are defined using a hierarchical framework that is very closely related to ours. Should future workers want to compare our net-to-gross values to data computed using either a different hierarchical framework or a different conceptual model altogether, we encourage reinterpretation of our stratigraphic data (see Appendix 1 and 2) and recalculation of net-to-gross values in the context of that framework or conceptual model to ensure that net-to-gross values can be assessed in a consistent way.

8. Conclusions

Analysis of deep-water slope channel fill and stacking patterns from the Tres Pasos Formation alongside data from subsurface slope systems yielded key insights into controls on the distribution of coarse-grained detritus along a slope. The abundance of sandstone-rich channel elements in downdip areas in the Tres Pasos Formation reveals that the degree of coarse-grained sediment bypass is a primary control on channel fill along a deep-water slope. It is concluded that the degree of coarse-grained sediment bypass that occurs at a given position on the slope is largely related to the gradient of the slope in that region; however, it is likely that turbidity current flow properties (e.g., grain size, flow size, sediment concentration) will also play a role in determining where coarse-grained sediment bypass will occur. For channel complexes and channel systems, sandstone proportion trends and stacking patterns are strongly linked to the topographic profile of the slope. It is predicted that channel complexes and channel systems that develop along slopes with smooth profiles will exhibit a systematic increase in sandstone proportion downdip, while complexes and systems that develop along slopes with irregular profiles will exhibit highly variable sandstone proportion trends downdip.

The compilation of net-to-gross data may offer a predictive template for assessment of reservoir volumes in analogous settings at various scales, which may aid with current natural resource exploration efforts. However, since net-to-gross values may not comprehensively capture variations in porosity and permeability within a subsurface reservoir, additional detailed analysis of geologic features that commonly affect porosity and permeability (e.g., grain size, proportion of matrix material, intra- and inter-reservoir unit architecture) is recommended for thorough characterization of reservoir connectivity wherever possible.

CRediT authorship contribution statement

Benjamin G. Daniels: Writing – review & editing, Writing – original draft, Visualization, Validation, Methodology, Investigation, Formal analysis, Data curation, Conceptualization. **Stephen M. Hubbard:** Writing – review & editing, Supervision, Project administration, Investigation, Funding acquisition, Formal analysis, Conceptualization. **Lisa Stright:** Writing – review & editing, Visualization, Validation, Investigation, Funding acquisition, Formal analysis, Data curation, Conceptualization. **Brian W. Romans:** Writing – review & editing, Visualization, Validation, Investigation, Funding acquisition, Formal analysis, Conceptualization.

Declaration of competing interest

The authors declare that they have no known competing financial interests or personal relationships that could have appeared to influence the work reported in this paper.

Data availability

All qualitative and quantitative data referenced in the manuscript text are presented in the figures, tables, and supplementary files that are associated with the manuscript.

Acknowledgements

Funding for this work was generously provided by the sponsors of the Chile Slope Systems Joint Industry Project (Anadarko, BHP Billiton,

Chevron, CNOOC, ConocoPhillips, Equinor, Hess, Repsol, and Shell), as well as via a Natural Sciences and Engineering Research Council of Canada (NSERC) Discovery Grant (RGPIN-2018-04223) to Hubbard, and by the University of Calgary Silver Anniversary Fellowship and Queen Elizabeth II graduate scholarships to Daniels. We wish to thank Mauricio Álvarez Kusanovic and Hella Roehrs Jeppesen, Armando Álvarez Saldivia, Jose Antonio Kusanovic and Tamara Mac Leod, Christian Cárdenas Alvarado, and Raúl Cárdenas Rodríguez for granting access to outcrops, as well as Tomislav Goic and Alejandrina Mac Leod for their support during our field work in Chile. We thank numerous current and former colleagues in the Chile Slope Systems Joint Industry Project, including Neal Auchter, Dustin Bauer, Daniel Bell, Rebecca Englert, Sean Fletcher, Allison Jackson, Sarah Jancuska, Sebastian Kaempfe-Droguett, Ryan Macauley, Casey Meirovitz, Paul Nesbit, Adam Nielson, Daniel Niquet, Erin Pemberton, Aaron Reimchen, and Sarah Southern, for assistance during field work and for lively discussions that helped clarify and refine ideas presented herein. We would also like to thank Schlumberger for providing a Petrel software license for use at the University of Calgary. Finally, we are grateful for comments and suggestions from Adam McArthur, Bryan Cronin, and Associate Editor Luca Colombera, which significantly improved the focus and clarity of an earlier version of this manuscript.

Appendices A-C. Supplementary data

Supplementary data to this article can be found online at https://doi.org/10.1016/j.marpetgeo.2024.106869.

References

Abreu, V., Sullivan, M., Pirmez, C., Mohrig, D., 2003. Lateral accretion packages (LAPs): an important reservoir element in deep water sinuous channels. Mar. Petrol. Geol. 20, 631–648.
Alpak, F.O., Barton, M.D., Naruk, S.J., 2013. The impact of fine-scale turbidite channel architecture on deep-water reservoir performance. AAPG Bull. 97, 251–284.
Armitage, D.A., Romans, B.W., Covault, J.A., Graham, S.A., 2009. The influence of mass-transport-deposit surface topography on the evolution of turbidite architecture: the Sierra Contreras, Tres Pasos Formation (Cretaceous), Southern Chile. J. Sediment. Res. 79, 287–301.
Armitage, D.A., McHargue, T., Fildani, A., Graham, S.A., 2012. Postavulsion channel evolution: Niger Delta continental slope. AAPG Bull. 96, 823–843.
Arnott, R.W.C., 2007. Stratal architecture and origin of lateral accretion deposits (LADs) and conterminous inner-bank levee deposits in a base-of-slope sinuous channel, lower Isaac Formation (Neoproterozoic), East-Central British Columbia, Canada. Mar. Petrol. Geol. 24, 515–528.
Auchter, N.C., Romans, B.W., Hubbard, S.M., 2016. Influence of deposit architecture on intrastratal deformation, slope deposits of the Tres Pasos Formation, Chile. Sediment. Geol. 341, 13–26.
Alves, T., 2015. Submarine slide blocks and associated soft-sediment deformation in deep-water basins: a review. Mar. Petrol. Geol. 67, 262–285.
Azpiroz-Zabala, M., Cartigny, M.J.B., Talling, P.J., Parsons, D.R., Sumner, E.J., Clare, M. A., Simmons, S.M., Cooper, C., Pope, E.L., 2017. Newly recognized turbidity current structure can explain prolonged flushing of submarine canyons. Sci. Adv. 3, e1700200.
Bain, H.A., Hubbard, S.M., 2016. Stratigraphic evolution of a long-lived submarine channel system in the late cretaceous nanaimo group, British columbia, Canada. Sediment. Geol. 337, 113–132.
Bakke, K., Petersen, S.A., Martinsen, O.J., Johansen, T.A., Lien, T., Thurmond, J., 2011. Seismic modeling of outcrop analogs: techniques and application. In: Martinsen, O. J., Pulham, A.J., Haughton, P.D.W., Sullivan, M.D. (Eds.), Outcrops Revitalized: Tools, Techniques and Applications, SEPM Concepts in Sedimentology and Paleontology, vol. 10, pp. 69–86.
Barton, M., O'Byrne, C., Pirmez, C., Prather, B., van der Vlugt, F., Alpak, F.O., Sylvester, Z., 2010. Turbidite channel architecture: recognizing and quantifying the distribution of channel base drapes using core and dipmeter data. In: Pöppelreiter, M., García-Carballido, C., Kraaijveld, M.A. (Eds.), Dipmeter and Borehole Image Log Technology, vol. 92. AAPG Memoir, pp. 195–210.
Bauer, D.B., Hubbard, S.M., Covault, J.A., Romans, B.W., 2020. Inherited depositional topography control on shelf-margin oversteepening, readjustment, and coarse-grained sediment delivery to deep water, Magallanes Basin, Chile. Front. Earth Sci. 7, 1–22.
Beaubouef, R.T., Rossen, C., Zelt, F.B., Sullivan, M.D., Mohrig, D.C., Jennette, D.C., 1999. Deep-water sandstones, Brushy Canyon Formation, west Texas. AAPG Continuing Education Course Notes 40.
Beaubouef, R.T., Friedmann, S.J., 2000. High resolution seismic/sequence stratigraphic framework for the evolution of Pleistocene intra slope basins, western Gulf of Mexico. In: Weimer, P., Slatt, R.M., Coleman, J., Rosen, N.C., Nelson, H., Bouma, A. H., Styzen, M.J., Lawrence, D. (Eds.), Deep-Water Reservoirs of the World. Gulf Coast Society–Society for Sedimentary Geology 20th Annual Research Conference, pp. 40–60.
Beaubouef, R.T., 2004. Deep-water leveed-channel complexes of the Cerro Toro Formation, Upper Cretaceous, southern Chile. AAPG Bull. 88, 1471–1500.
Bell, D., Kane, I.A., Pontén, A.S.M., Flint, S.S., Hodgson, D.M., Barrett, B.J., 2018. Spatial variability in depositional reservoir quality of deep-water channel-fill and lobe deposits. Mar. Petrol. Geol. 98, 97–115.
Bell, D., Hodgson, D.M., Pontén, A.S.M., Hansen, L.A.S., Flint, S.S., Kane, I.A., 2020. Stratigraphic hierarchy and three-dimensional evolution of an exhumed submarine slope channel system. Sedimentology 67, 3259–3289.
Bouma, A.H., 1962. Sedimentology of Some Flysch Deposits: A Graphic Approach to Facies Interpretation. Elsevier, Amsterdam, p. 168.
Bozetti, G., Kneller, B., Cronin, B.T., Li, P., McArthur, A., Xu, J., 2023. Lateral and temporal variations of a multi-phase coarse-grained submarine slope channel system, Upper Cretaceous Cerro Toro Formation, southern Chile. J. Sediment. Res. 93, 161–186.
Calderón, M., Hervé, F., Fuentes, F., Fosdick, J.C., Sepúlveda, F., Galaz, G., 2016. Tectonic evolution of the Mesozoic Andean Metamorphic Complexes and the Rocas Verdes ophiolites in southern Patagonia. In: Ghiglione, M.C. (Ed.), Geodynamic Evolution of the Southernmost Andes. Springer International Publishing, pp. 7–36.
Cartigny, M.J.B., Ventra, D., Postma, G., van Den Berg, J.H., 2014. Morphodynamics and sedimentary structures of bedforms under supercritical-flow conditions: new insights from flume experiments. Sedimentology 61, 712–748.
Catterall, V., Redfern, J., Gawthorpe, R., Hansen, D., Thomas, M., 2010. Architectural style and quantification of a submarine channel-levee system location in a structurally complex area: offshore Nile Delta. J. Sediment. Res. 80, 991–1017.
Çelik, H., Cronin, B., 2020. Controls on deep-water slope channel complex fill, propagation, stacking, and orientation in the Middle Eocene-Oligocene Kırkgeçit Formation, Elazığ, eastern Turkey. Turkish J. Earth Sci. 29, 976–1003.
Clark, J.D., Pickering, K.T., 1996. Architectural elements and growth patterns of submarine channels: application to hydrocarbon exploration. AAPG Bull. 80, 194–220.
Covault, J.A., Romans, B.W., Graham, S.A., 2009. Outcrop expression of a continental-margin-scale shelf-edge delta from the Cretaceous Magallanes Basin, Chile. J. Sediment. Res. 79, 523–539.
Covault, J.A., Shelef, E., Traer, M., Hubbard, S.M., Romans, B.W., Fildani, A., 2012. Deep-water channel run-out length: insights from seafloor geomorphology. J. Sediment. Res. 82, 21–36.
Covault, J.A., Sylvester, Z., Hubbard, S.M., Jobe, Z.R., Sech, R.P., 2016. The stratigraphic record of submarine-channel evolution. Sediment. Rec. 14, 4–11.
Crisóstomo-Figueroa, A., McArthur, A.D., Dorrell, R.M., Amy, L., McCaffrey, W.D., 2021. A new modelling approach to sediment bypass prediction applied to the East Coast Basin, New Zealand. Geol. Soc. Am. Bull. 133, 1734–1748.
Cronin, B.T., and the Jubilee Team, Tullow Ghana Limited, 2022. Giant pockmark-initiated deep-water slope channel complexes. AAPG Bull. 106, 829–868.
Cross, N.E., Cunningham, A., Cook, R.J., Taha, A., Esmaie, E., El Swidan, N., 2009. Three-dimensional seismic geomorphology of a deep-water slope-channel system: the Sequoia field, offshore west Nile Delta, Egypt. AAPG Bull. 93, 1063–1086.
Cullis, S., Colombera, L., Patacci, M., McCaffrey, W.D., 2018. Hierarchical classifications of the sedimentary architecture of deep-marine depositional systems. Earth Sci. Rev. 179, 38–71.
Dailly, P., Henderson, T., Hudgens, E., Kanschat, K., Lowrey, P., 2012. Exploration for Cretaceous stratigraphic traps in the gulf of Guinea, West Africa and the discovery of the Jubilee Field: a play opening discovery in the Tano Basin, offshore Ghana. Geol. Soc. London Spec. Pub. 369, 235–248.
Dalziel, I.W.D., de Wit, M.J., Palmer, K.F., 1974. Fossil marginal basin in the southern Andes. Nature 250, 291–294.
Daniels, B.G., Auchter, N.C., Hubbard, S.M., Romans, B.W., Matthews, W.A., Stright, L., 2018. Timing of deep-water slope evolution constrained by large-n detrital and volcanic ash zircon geochronology, Cretaceous Magallanes Basin, Chile. Geol. Soc. Am. Bull. 130, 438–454.
Daniels, B.G., Hubbard, S.M., Romans, B.W., Malkowski, M.A., Matthews, W.A., Bernhardt, A., Kaempfe, S.A., Jobe, Z.R., Fosdick, J.C., Schwartz, T.M., Fildani, A., Graham, S.A., 2019. Revised chronostratigraphic framework for the cretaceous Magallanes-Austral Basin, última esperanza province, Chile. J. S. Am. Earth Sci. 94, 102209.
de Wit, M.J., Stern, C.R., 1981. Variations in the degree of crustal extension during formation of a back-arc basin. Tectonophysics 72, 229–260.
Deptuck, M.E., Steffens, G.S., Barton, M., Pirmez, C., 2003. Architecture and evolution of upper fan channel-belts on the Niger Delta slope and in the Arabian Sea. Mar. Petrol. Geol. 20, 649–676.
Deptuck, M.E., Sylvester, Z., Pirmez, C., O'Byrne, C., 2007. Migration-aggradation history and 3-D seismic geomorphology of submarine channels in the Pleistocene Benin-major Canyon, western Niger Delta slope. Mar. Petrol. Geol. 24, 406–433.
Di Celma, C.N., Brunt, R.L., Hodgson, D.M., Flint, S.S., Kavanagh, J.P., 2011. Spatial and temporal evolution of a Permian submarine slope channel-levee system, Karoo Basin, South Africa. J. Sediment. Res. 81, 579–599.
Englert, R.G., Hubbard, S.M., Coutts, D.S., Matthews, W.A., 2018. Tectonically controlled initiation of contemporaneous deep-water channel systems along a Late Cretaceous continental margin, western British Columbia, Canada. Sedimentology 65, 2404–2438.
Englert, R.G., Hubbard, S.M., Matthews, W.A., Coutts, D.S., Covault, J.A., 2020. The evolution of submarine slope-channel systems: timing of incision, bypass, and aggradation in Late Cretaceous Nanaimo Group channel-system strata, British Columbia, Canada. Geosphere 16, 281–296.

Englert, R.G., Hubbard, S.M., Cartigny, M.J.B., Clare, M.A., Coutts, D.S., Hage, S., Hughes Clarke, J., Jobe, Z., Lintern, D.G., Stacey, C., Vendettuoli, D., 2021. Quantifying the three-dimensional stratigraphic expression of cyclic steps by integrating seafloor and deep-water outcrop observations. Sedimentology 68, 1465–1501.
Flint, S.S., Hodgson, D.M., Sprague, A.R., Brunt, R.L., Van der Merwe, W.C., Figueiredo, J., Prélat, A., Box, D., Di Celma, C., Kavanagh, J.P., 2011. Depositional architecture and sequence stratigraphy of the Karoo basin floor to shelf edge succession, Laingsburg depocentre, South Africa. Mar. Petrol. Geol. 28, 658–674.
Fildani, A., Hessler, A.M., 2005. Stratigraphic record across a retroarc basin inversion: Rocas verdes–magallanes basin, patagonian andes. Geol. Soc. Am. Bull. 117, 1596–1614.
Fildani, A., Hubbard, S.M., Covault, J.A., Maier, K.L., Romans, B.W., Traer, M., Rowland, J.C., 2013. Erosion at inception of deep-sea channels. Mar. Petrol. Geol. 41, 48–61.
Fosdick, J.C., Graham, S.A., Hilley, G.E., 2014. Influence of attenuated lithosphere and sediment loading on flexure of the deep-water Magallanes retroarc foreland basin, Southern Andes. Tectonics 33, 2505–2525.
Fowler, J.N., Novakovic, L., 2018. Deepwater slope valley reservoir architecture and connectivity, Brazil. Lead. Edge 37, 276–282.
Frey-Martínez, J., Cartwright, J., James, D., 2006. Frontally confined versus frontally emergent submarine landslides: a 3D seismic characterisation. Mar. Petrol. Geol. 23, 585–604.
Gardner, M.H., Borer, J.M., Melick, J.J., Mavilla, N., Dechesne, M., Wagerle, R.N., 2003. Stratigraphic process-response model for submarine channels and related features from studies of Permian Brushy Canyon outcrops, West Texas. Mar. Petrol. Geol. 20, 757–787.
Gee, M.J.R., Gawthorpe, R.L., 2006. Submarine channels controlled by salt tectonics: examples from 3D seismic data, offshore Angola. Mar. Petrol. Geol. 23, 443–458.
Greenlee, S.M., Devlin, W.J., Miller, K.G., Mountain, G.S., Flemings, P.B., 1992. Integrated sequence stratigraphy of Neogene deposits, New Jersey continental shelf and slope: comparison with the Exxon model. Geol. Soc. Am. Bull. 104, 1403–1411.
Hage, S., Cartigny, M.J.B., Clare, M.A., Sumner, E.J., Vendettuoli, D., Hughes Clarke, J. E., Hubbard, S.M., Talling, P.J., Lintern, D.G., Stacey, C.D., Englert, R.G., Vardy, M. E., Hunt, J.E., Yokokawa, M., Parsons, D.R., Hizzett, J.L., Azpiroz-Zabala, M., Vellinga, A.J., 2018. How to recognize crescentic bedforms formed by supercritical turbidity currents in the geologic record: insights from active submarine channels. Geology 46, 563–566.
Hampton, M.A., 1972. The role of subaqueous debris flow in generating turbidity currents. J. Sediment. Res. 42, 775–793.
Hansen, L.A.S., Callow, R.H.T., Kane, I., Gamberi, F., Rovere, M., Cronin, B.T., Kneller, B., 2015. Genesis and character of thin-bedded turbidites associated with submarine channels. Mar. Petrol. Geol. 67, 852–879.
Hansen, L.A.S., Hodgson, D.M., Pontén, A., Bell, D., Flint, S., 2019. Quantification of basin-floor fan pinchouts: examples from the Karoo Basin, South Africa. Front. Earth Sci. 7, 1–20.
Heijnen, M.S., Clare, M.A., Cartigny, M.J.B., Talling, P.J., Hage, S., Pope, E.L., Bailey, L., Sumner, E., Lintern, D.G., Stacey, C., Parsons, D.R., Simmons, S.M., Chen, Y., Hubbard, S.M., Eggenhuisen, J.T., Kane, I., Hughes Clarke, J.E., 2022. Fill, flush or shuffle: how is sediment carried through submarine channels to build lobes? Earth Planet Sci. Lett. 584, 117481.
Heiniö, P., Davies, R.J., 2007. Knickpoint migration in submarine channels in response to fold growth, western Niger Delta. Mar. Petrol. Geol. 24, 434–449.
Hiscott, R.N., Hall, F.R., Pirmez, C., 1997. Turbidity current overspill from the Amazon Channel: texture of the silt/sand load, palaeoflow from anisotropy of magnetic susceptibility, and implications for flow processes. Proc. ODP Sci. Results 155, 53–78.
Hodgson, D.M., Di Celma, C.N., Brunt, R.L., Flint, S.S., 2011. Submarine slope degradation and aggradation and the stratigraphic evolution of channel-levee systems. J. Geol. Soc. London 168, 625–628.
Houseknecht, D.W., Bird, K.J., Schenk, C.J., 2009. Seismic analysis of clinoform depositional sequences and shelf-margin trajectories in Lower Cretaceous (Albian) strata, Alaska North Slope. Basin Res. 21, 644–654.
Hubbard, S.M., Romans, B.W., Graham, S.A., 2008. Deep-water foreland basin deposits of the Cerro Toro Formation, Magallanes Basin, Chile: architectural elements of a sinuous basin axial channel belt. Sedimentology 55, 1333–1359.
Hubbard, S.M., de Ruig, M.J., Graham, S.A., 2009. Confined channel-levee complex development in an elongate depo-center: deep-water Tertiary strata of the Austrian Molasse basin. Mar. Petrol. Geol. 26, 85–112.
Hubbard, S.M., Fildani, A., Romans, B.W., Covault, J.A., McHargue, T.R., 2010. High-relief slope clinoform development: insights from outcrop, Magallanes Basin, Chile. J. Sediment. Res. 80, 357–375.
Hubbard, S.M., Covault, J.A., Fildani, A., Romans, B.W., 2014. Sediment transfer and deposition in slope channels: deciphering the record of enigmatic deep-sea processes from outcrop. Geol. Soc. Am. Bull. 126, 857–871.
Hubbard, S.M., Jobe, Z.R., Romans, B.W., Covault, J.A., Sylvester, Z., Fildani, A., 2020. The stratigraphic evolution of a submarine channel: linking seafloor dynamics to depositional products. J. Sediment. Res. 90, 673–686.
Hübscher, C., Spieß, V., Breitzke, M., Weber, M.E., 1997. The youngest channel-levee system of the Bengal Fan: results from digital sediment echosounder data. Mar. Geol. 141, 125–145.
Hughes Clarke, J.E., 2016. First wide-angle view of channelized turbidity currents links migrating cyclic steps to flow characteristics. Nat. Commun. 7, 1–13.
Jackett, S., Jobe, Z.R., Lutz, B.P., Da Gama, R.O.B.P., Sylvester, Z., Prince, I.M., Albrecht, H.L., Prasad, T., 2014. Detecting baffle mudstones using microfossils: an integrated working example from the Cardamom Field, Block 427 Garden Banks, Gulf of Mexico. Palaeogeogr. Palaeoclimatol. Palaeoecol. 413, 133–143.
Jackson, A., Stright, L., Hubbard, S.M., Romans, B.W., 2019. Static connectivity of stacked deep-water channel elements constrained by high-resolution digital outcrop models. AAPG Bull. 103, 2943–2973.
Janocko, M., Nemec, W., Henriksen, S., Warchoł, M., 2013. The diversity of deep-water sinuous channel belts and slope valley-fill complexes. Mar. Petrol. Geol. 41, 7–34.
Jobe, Z.R., Lowe, D.R., Uchytil, S.J., 2011. Two fundamentally different types of submarine canyons along the continental margin of Equatorial Guinea. Mar. Petrol. Geol. 28, 843–860.
Jobe, Z.R., Sylvester, Z., Parker, A.O., Howes, N., Slowey, N., Pirmez, C., 2015. Rapid adjustment of submarine channel architecture to changes in sediment supply. J. Sediment. Res. 85, 729–753.
Kane, I.A., Kneller, B.C., Dykstra, M., Kassem, A., McCaffrey, W.D., 2007. Anatomy of a submarine channel-levee: an example from Upper Cretaceous slope sediments, Rosario Formation, Baja California, Mexico. Mar. Petrol. Geol. 24, 540–563.
Kane, I.A., Hodgson, D.M., 2011. Sedimentological criteria to differentiate submarine channel levee subenvironments: exhumed examples from the Rosario Fm. (Upper Cretaceous) of Baja California, Mexico, and the Fort Brown Fm. (Permian), Karoo Basin, S. Africa. Mar. Petrol. Geol. 28, 807–823.
Katz, H.R., 1963. Revision of cretaceous stratigraphy in Patagonian Cordillera of Ultima Esperanza, Magallanes Province, Chile. AAPG Bull. 47, 506–524.
Kendell, K.L., 2012. Variations in salt expulsion style within the Sable Canopy Complex, central Scotian margin. Can. J. Earth Sci. 49, 1504–1522.
Kneller, B., Dykstra, M., Fairweather, L., Milana, J.P., 2016. Mass-transport and slope accommodation: implications for turbidite sandstone reservoirs. AAPG Bull. 100, 213–235.
Kneller, B., Bozetti, G., Callow, R., Dykstra, M., Hansen, L., Kane, I., Li, P., McArthur, A., Catharina, A.S., Dos Santos, T., Thompson, P., 2020. Architecture, process, and environmental diversity in a late Cretaceous slope channel system. J. Sediment. Res. 90, 1–26.
Labourdette, R., 2007. Integrated three-dimensional modeling approach of stacked turbidite channels. AAPG Bull. 91, 1603–1618.
Labourdette, R., Bez, M., 2010. Element migration in turbidite systems: random or systematic depositional processes? AAPG Bull. 94, 345–368.
Li, P., Kneller, B.C., Hansen, L., Kane, I.A., 2016. The classical turbidite outcrop at San Clemente, California revisited: an example of sandy submarine channels with asymmetric facies architecture. Sediment. Geol. 346, 1–16.
Lowe, D.R., 1982. Sediment gravity flows; II, depositional models with special reference to the deposits of high-density turbidity currents. J. Sediment. Res. 52, 279–297.
Ma, H.-X., Fan, G.Z., Shao, D.-L., Ding, L.-B., Sun, H., Zhang, Y., Zhang, Y.-G., Cronin, B. T., 2020. Deep-water depositional architecture and sedimentary evolution in the Rakhine Basin, northeast Bay of Bengal. Petrol. Sci. 17, 598–614.
Macauley, R.V., Hubbard, S.M., 2013. Slope channel sedimentary processes and stratigraphic stacking, Cretaceous Tres Pasos Formation slope systems, Chilean Patagonia. Mar. Petrol. Geol. 41, 146–162.
Macellari, C.E., Barrio, C.A., Manassero, M.J., 1989. Upper Cretaceous to Paleocene depositional sequences and sandstone petrography of southwestern Patagonia (Argentina and Chile). J. S. Am. Earth Sci. 2, 223–239.
Malkowski, M.A., Sharman, G.R., Graham, S.A., Fildani, A., 2017. Characterisation and diachronous initiation of coarse clastic deposition in the Magallanes-Austral foreland basin, Patagonian Andes. Basin Res. 29, 298–326.
Mayall, M., Kneller, B., 2021. Seismic interpretation workflows for deep-water systems: a practical guide for the subsurface. AAPG Bull. 105, 2127–2157.
Mayall, M., Jones, E., Casey, M., 2006. Turbidite channel reservoirs-Key elements in facies prediction and effective development. Mar. Petrol. Geol. 23, 821–841.
McHargue, T., Pyrcz, M.J., Sullivan, M.D., Clark, J.D., Fildani, A., Romans, B.W., Covault, J.A., Levy, M., Posamentier, H.W., Drinkwater, N.J., 2011. Architecture of turbidite channel systems on the continental slope: patterns and predictions. Mar. Petrol. Geol. 28, 728–743.
Meirovitz, C.D., Stright, L., Hubbard, S.M., Romans, B.W., 2020. The influence of inter- and intra-channel architecture on deep-water turbidite reservoir performance. Petrol. Geosci. 27 petgeo2020-005.
Middleton, G.V., Hampton, M.A., 1973. Sediment gravity flows: mechanics of flow and deposition. In: Middleton, G.V., Bouma, A.H. (Eds.), Turbidites and Deep Water Sedimentation. SEPM Pacific Section Short Course Notes, pp. 1–38.
Middleton, G.V., Hampton, M.A., 1976. Subaqueous sediment transport and deposition by sediment gravity flows. In: Stanley, D.J., Swift, D.J.P. (Eds.), Marine Sediment Transport and Environmental Management. Wiley, New York, pp. 197–218.
Mokhtar, M., Saad, M., Selim, S., 2016. Reservoir architecture of deep marine slope channel, Scarab field, offshore Nile Delta, Egypt: application of reservoir characterization. Egypt J. Petrol. 25, 495–508.
Morris, E.A., Hodgson, D.M., Flint, S.S., Brunt, R.L., Butterworth, P.J., Verhaeghe, J., 2014. Sedimentology, stratigraphic architecture, and depositional context of submarine frontal-lobe complexes. J. Sediment. Res. 84, 763–780.
Moscardelli, L., Wood, L., Mann, P., 2006. Mass-transport complexes and associated processes in the offshore area of Trinidad and Venezuela. AAPG Bull. 90, 1059–1088.
Mutti, E., 1992. Turbidite sandstones. San Donato, Milanese, Università di Parma, Agip 275.
Mutti, E., Normark, W.R., 1987. Comparing examples of modern and ancient turbidite systems: problems and concepts. In: Legget, J.K., Zuffa, G.G. (Eds.), Deep Water Clastic Deposits: Models and Case Histories. Graham and Trotman, London, pp. 1–38.

Mutti, E., Normark, W.R., 1991. An integrated approach to the study of turbidite systems. In: Weimer, P., Link, M.H. (Eds.), Seismic Facies and Sedimentary Processes of Submarine Fans and Turbidite Systems. Springer Verlag, New York, pp. 75–106.
Nesbit, P.R., Hubbard, S.M., Daniels, B.G., Bell, D., Englert, R.G., Hugenholtz, C.H., 2021. Digital re-evaluation of down-dip channel-fill architecture in deep-water slope deposits: multi-scale perspectives from UAV-SfM. The Depositional Record 7, 480–499.
Peakall, J., McCaffrey, W.D., Kneller, B.C., 2000. A process model for the evolution, morphology, and architecture of sinuous submarine channels. J. Sediment. Res. 70, 434–448.
Pemberton, E.A.L., Hubbard, S.M., Fildani, A., Romans, B.W., Stright, L., 2016. The stratigraphic expression of decreasing confinement along a deep-water sediment routing system: outcrop example from southern Chile. Geosphere 12, 114–134.
Pemberton, E.A.L., Stright, L., Fletcher, S., Hubbard, S.M., 2018. The influence of stratigraphic architecture on seismic response: reflectivity modeling of outcropping deepwater channel units. Interpretation 6, T783–T808.
Pickering, K.T., Cantalejo, B., 2015. Deep-marine environments of the Middle Eocene Upper Hecho group, Spanish Pyrenees: introduction. Earth Sci. Rev. 144, 1–9.
Pickering, K.T., Clark, J.D., Smith, R.D.A., Hiscott, R.N., Ricci Lucchi, F., Kenyon, N.H., 1995. Architectural element analysis of turbidite systems, and selected topical problems for sand-prone deep-water systems. In: Pickering, K.T., Hiscott, R.N., Kenyon, N.H., Ricci Lucchi, F., Smith, R.D.A. (Eds.), Atlas of Deep Water Environments: Architectural Style in Turbidite Systems. Chapman and Hall, London, pp. 1–10.
Piper, D.J.W., Normark, W.R., 2001. Sandy fans-from Amazon to Hueneme and beyond. AAPG Bull. 85, 1407–1438.
Pirmez, C., Flood, R.D., 1995. Morphology and structure of Amazon Channel. Proc. ODP Init. Rep. 155, 23–45.
Pirmez, C., Hiscott, R.N., Kronen, J.D., 1997. Sandy turbidite successions at the base of channel-levee systems of the Amazon Fan revealed by FMS logs and cores: unraveling the facies architecture of large submarine fans. Proc. ODP Sci. Results 155, 7–34.
Plink-Björklund, P., Mellere, D., Steel, R.J., 2001. Turbidite variability and architecture of sand-prone deep-water slopes: Eocene clinoforms in the Central Basin, Spitsbergen. J. Sediment. Res. 71, 895–912.
Pope, E.L., Cartigny, M.J.B., Clare, M.A., Talling, P.J., Lintern, D.G., Vellinga, A., Hage, S., Açikalin, S., Bailey, L., Chapplow, N., Chen, Y., Eggenhuisen, J.T., Hendry, A., Heerema, C.J., Heijnen, M.S., Hubbard, S.M., Hunt, J.E., McGhee, C., Parsons, D.R., Simmons, S.M., Stacey, C.D., Vendettuoli, D., 2022. First source-to-sink monitoring shows dense head controls sediment flux and runout in turbidity currents. Sci. Adv. 8, eabj3220.
Porter, N.L., Sprague, A.R.G., Sullivan, M.D., Jennette, D.C., Beaubouef, R.T., Garfield, T. R., Rossen, C., Sickafoose, D.K., Jensen, G.N., Friedmann, S.J., Mohrig, D.C., 2006. Stratigraphic organization and predictability of mixed coarse- and fine-grained lithofacies successions in a Lower Miocene deep-water slope-channel system, Angola Block 15. In: Harris, P.M., Weber, L.J. (Eds.), Giant Hydrocarbon Reservoirs of the World: from Rocks to Reservoir Characterization and Modeling, AAPG Bull, vol. 88, pp. 281–306.
Posamentier, H.W., Kolla, V., 2003. Seismic geomorphology and stratigraphy of depositional elements in deep-water settings. J. Sediment. Res. 73, 367–388.
Pyles, D.R., Jennette, D.C., Tomasso, M., Beaubouef, R.T., Rossen, C., 2010. Concepts learned from a 3D outcrop of a sinuous slope channel complex: Beacon Channel Complex, Brushy Canyon Formation, West Texas, U.S.A. J. Sediment. Res. 80, 67–96.
Pyles, D.R., Strachan, L.J., Jennette, D.C., 2014. Lateral juxtapositions of channel and lobe elements in distributive submarine fans: three-dimensional outcrop study of the Ross Sandstone and geometric model. Geosphere 10, 1104–1122.
Qin, Y., Alves, T.M., Constantine, J., Gamboa, D., 2016. Quantitative seismic geomorphology of a submarine channel system in SE Brazil (Espírito Santo Basin): Scale comparison with other submarine channel systems. Mar. Petrol. Geol. 78, 455–473.
Reguzzi, S., Marini, M., Felletti, F., El Kati, I., Zuffetti, C., Tabyaoui, H., 2023. Stratigraphic evolution of a spectacularly exposed turbidite channel belt from the Tachrift System (late Tortonian, north-East Morocco). Sedimentology 70, 1075–1109.
Reimchen, A.P., Hubbard, S.M., Stright, L., Romans, B.W., 2016. Using sea-floor morphometrics to constrain stratigraphic models of sinuous submarine channel systems. Mar. Petrol. Geol. 77, 92–115.
Romans, B.W., Graham, S.A., 2013. A deep-time perspective of land-ocean linkages in the sedimentary record. Ann. Rev. Mar. Sci 5, 69–94.
Romans, B.W., Fildani, A., Hubbard, S.M., Covault, J.A., Fosdick, J.C., Graham, S.A., 2011. Evolution of deep-water stratigraphic architecture, Magallanes Basin, Chile. Mar. Petrol. Geol. 28, 612–628.
Saller, A.H., Dharmasamadhi, I.N.W., 2012. Controls on the development of valleys, canyons, and unconfined channel-levee complexes on the Pleistocene Slope of East Kalimantan, Indonesia. Mar. Petrol. Geol. 29, 15–34.
Saller, A.H., Noah, J.T., Prama Ruzuar, A., Schneider, R., 2004. Linked lowstand delta to basin-floor fan deposition, offshore Indonesia: An analog for deep-water reservoir systems. AAPG Bull. 88, 21–46.
Saller, A.H., Dharmasamadhi, I.N.W., Lilburn, T., Earley, R., 2010. Seismic geomorphology of submarine slopes: channel-levee complexes versus slope valleys and canyon, Pleistocene, East Kalimantan, Indonesia. In: Wood, L.J., Simo, T.T., Rosen, N.C. (Eds.), Seismic Imaging of Depositional and Geomorphic Systems, vol. 30. SEPM Spec. Publ., pp. 433–471
Samuel, A., Kneller, B., Raslan, S., Sharp, A., Parsons, C., 2003. Prolific deep-marine slope channels of the Nile Delta, Egypt. AAPG Bull. 87, 541–560.
Sansom, P., 2018. Hybrid turbidite-contourite systems of the Tanzanian margin. Petrol. Geosci. 24, 258–276.
Schlumberger, 2014. Petrel E&P Software Platform. Schlumberger Limited, Houston, Texas. https://www.software.slb.com/products/petrel.
Schwartz, T.M., Graham, S.A., 2015. Stratigraphic architecture of a tide-influenced shelf-edge delta, Upper Cretaceous Dorotea Formation, Magallanes-Austral Basin, Patagonia. Sedimentology 62, 1039–1077.
Smith, C.H.L., 1977. Sedimentology of the Late Cretaceous (Santonian–Maastrichtian) Tres Pasos Formation, Ultima Esperanza District, Southern Chile. University of Wisconsin,. Unpublished M.S. thesis,.
Sprague, A.R., Sullivan, M.D., Campion, K.M., Jensen, G.N., Goulding, F.J., Sickafoose, D.K., Jennette, D.C., 2002. The physical stratigraphy of deep-water strata: a hierarchical approach to the analysis of genetrically related elements for improved reservoir prediction. In: AAPG Annual Meeting Programs with Abstracts (Houston, Texas).
Sprague, A.R., Garfield, T.R., Goulding, F.J., Beaubouef, R.T., Sullivan, M.D., Rossen, C., Campion, K.M., Sickafoose, D.K., Abreu, V., Schellpeper, M.E., Jensen, G.N., Jennette, D.C., Pirmez, C., Dixon, B.T., Ying, D., Ardill, J., Mohrig, D.C., Porter, M.L., Farrell, M.E., Mellere, D., 2005. Integrated slope channel depositional models: the key to successful prediction of reservoir presence and quality in offshore West Africa. In: CIPM, Cuarto EExitep 2005 (Veracruz, Mexico).
Steel, E., Buttles, J., Simms, A.R., Mohrig, D., Meiburg, E., 2017. The role of buoyancy reversal in turbidite deposition and submarine fan geometry. Geology 45, 35–38.
Stevenson, C.J., Jackson, C.A.L., Hodgson, D.M., Hubbard, S.M., Eggenhuisen, J.T., 2015. Deep-water sediment bypass. J. Sediment. Res. 85, 1058–1081.
Straub, K.M., Mohrig, D., Buttles, J., McElroy, B., Pirmez, C., 2011. Quantifying the influence of channel sinuosity on the depositional mechanics of channelized turbidity currents: A laboratory study. Mar. Petrol. Geol. 28, 744–760.
Sullivan, M., Jensen, G., Goulding, F., Jennette, D., Foreman, L., Stern, D., 2000. Architectural analysis of deep-water outcrops: Implications for exploration and development of the Diana sub-basin, western Gulf of Mexico. In: Weimer, P., Slatt, R. M., Coleman, J., Rosen, N.C., Nelson, H., Bouma, A.H., Styzen, M.J., Lawrence, D.T. (Eds.), Deep-Water Reservoirs of the World. Gulf Coast Society–Society for Sedimentary Geology 20th Annual Research Conference, pp. 1010–1031.
Sylvester, Z., Deptuck, M.E., Prather, B.E., Pirmez, C., O'Byrne, C., 2012. Seismic stratigraphy of a shelf-edge delta and linked submarine channels in the northeastern Gulf of Mexico. In: Prather, B.E., Deptuck, M.E., Mohrig, D., Van Hoorn, B., Wynn, R. B. (Eds.), Application of the Principles of Seismic Geomorphology to Continental-Slope and Base-Of-Slope Systems: Case Studies from Seafloor to Near-Seafloor Analogues, vol. 99. SEPM Spec. Publ., pp. 31–59
Symons, W.O., Sumner, E.J., Talling, P.J., Cartigny, M.J.B., Clare, M.A., 2016. Large-scale sediment waves and scours on the modern seafloor and their implications for the prevalence of supercritical flows. Mar. Geol. 371, 130–148.
Talling, P.J., Masson, D.G., Sumner, E.J., Malgesini, G., 2012. Subaqueous sediment density flows: depositional processes and deposit types. Sedimentology 59, 1937–2003.
Tek, D.E., Poyatos-Moré, M., Patacci, M., McArthur, A.D., Colombera, L., Cullen, T.M., McCaffrey, W.D., 2020. Syndepositional tectonics and mass-transport deposits control channelized, bathymetrically complex deep-water systems (Aínsa depocenter, Spain). J. Sediment. Res. 90, 729–762.
Vendettuoli, D., Clare, M.A., Hughes Clarke, J.E., Vellinga, A., Hizzet, J., Hage, S., Cartigny, M.J.B., Talling, P.J., Waltham, D., Hubbard, S.M., Stacey, C., Lintern, D.G., 2019. Daily bathymetric surveys document how stratigraphy is built and its extreme incompleteness in submarine channels. Earth Planet Sci. Lett. 515, 231–247.
Ward, N.I.P., Alves, T.M., Blenkinsop, T.G., 2018. Submarine sediment routing over a blocky mass-transport deposit in the Espírito Santo Basin, SE Brazil. Basin Res. 30, 816–834.
Xu, J.P., Barry, J.P., Paull, C.K., 2013. Small-scale turbidity currents in a big submarine canyon. Geology 41, 143–146.
Zhang, J., Wu, S., Hu, G., Fan, T., Lin, Y., Fan, H., Jiang, L., Lin, P., 2018. Application of four-dimensional monitoring to understand reservoir heterogeneity controls on fluid flow during the development of a submarine channel system. AAPG Bull. 102, 2017–2044.